THE DESIGN AND PRODUCTION OF INTERFERENCE EDGE FILTERS WITH PLASMA ION ASSISTED DEPOSITION TECHNIQUE FOR A SPACE CAMERA

A THESIS SUBMITTED TO
THE GRADUATE SCHOOL OF NATURAL AND APPLIED SCIENCES
OF
MIDDLE EAST TECHNICAL UNIVERSITY

BY

BURCU BARUTÇU

IN PARTIAL FULFILLMENT OF THE REQUIREMENTS
FOR
THE DEGREE OF MASTER OF SCIENCE
IN
PHYSICS

AUGUST 2012

Approval of the thesis:

THE DESIGN AND PRODUCTION OF INTERFERENCE EDGE FILTERS WITH PLASMA ION ASSISTED DEPOSITION TECHNIQUE FOR A SPACE CAMERA

submitted by **BURCU BARUTÇU** in partial fulfillment of the requirements for the degree of **Master of Science in Physics Department, Middle East Technical University** by,

Prof. Dr. Canan Özgen
Dean, Graduate School of **Natural and Applied Sciences** ________________

Prof. Dr. Mehmet T. Zeyrek
Head of Department, **Physics** ________________

Assoc. Prof. Dr. Akif Esendemir
Supervisor, **Physics Department** ________________

Examining Committee Members:

Prof. Dr. Mehmet Parlak
Physics Dept., METU ________________

Assoc. Prof. Dr. Akif Esendemir
Physics Dept., METU ________________

Assoc. Prof. Dr. Enver Bulur
Physics Dept., METU ________________

Assit. Prof. Dr. Sinan Kaan Yerli
Physics Dept., METU ________________

Assoc. Prof. Dr. H. Gül Yağlıoğlu
Physics Engineering Dept., Ankara University ________________

Date: ________________

I hereby declare that all information in this document has been obtained and presented in accordance with academic rules and ethical conduct. I also declare that, as required by these rules and conduct, I have fully cited and referenced all material and results that are not original to this work.

Name, Last Name: BURCU BARUTÇU

Signature :

ABSTRACT

THE DESIGN AND PRODUCTION OF INTERFERENCE EDGE FILTERS WITH PLASMA ION ASSISTED DEPOSITION TECHNIQUE FOR A SPACE CAMERA

Barutçu, Burcu
M.Sc., Department of Physics
Supervisor : Assoc. Prof. Dr. Akif Esendemir

August 2012, 78 pages

Interference filters are multilayer thin film devices. They use interference effects between the incident and reflected radiation waves at each layer interface to select wavelengths. The production of interference filters depend on the precise deposition of thin material layers on substrates which have suitable optical properties. In this thesis, the main target is to design and produce two optical filters (short-pass filter and long-pass filter) for the CCDs that will be used in the electronics of a space camera. By means of these filters, it is possible to take image in different bands (RGB and NIR) by identical two CCDs. The filters will be fabricated by plasma ion-assisted deposition technique.

Keywords: Interference Filter, Optical Coating, Thin Film, Deposition Techniques, PVD (Physical Vapor Deposition), CCD (Charge-Coupled Devices), Transmission, Reflection, OptiLayer

ÖZ

BİR UYDU KAMERASINDA KULLANILACAK GİRİŞİM FİLTRELERİNİN TASARIMI VE PLAZMA IYON DESTEKLİ KAPLAMA TEKNİĞİ ILE ÜRETİMİ

Barutçu, Burcu
Yüksek Lisans, Fizik Bölümü
Tez Yöneticisi : Doç. Dr. Akif Esendemir

Ağustos 2012, 78 sayfa

Girişim filtreleri çok katmanlı ince film yapılardır. Dalga boylarını seçmek için, her arayüzde gerçekleşen, gelen ve yansıyan radyasyon dalgaları arasındaki girişim olayını kullanırlar. Girişim filtrelerinin üretimi, uygun optik özelliklere sahip olan alt tabakaların üzerine ince malzeme tabakalarının hassas depozisyonuna dayanır. Bu tez, bir uzay kamerasının elektroniğindeki CCDlerin üzerinde kullanılmak üzere iki optik filtre (kısa dalga geçiren filtre ve uzun dalga geçiren filtre) tasarımını ve üretimini içermektedir. Bu filtreler sayesinde aynı tip iki CCD ile farklı bantlarda (RGB ve NIR) görüntü alabilmek mümkün olmaktadır. Filtreler plazma-iyon destekli kaplama yöntemi ile üretilecektir.

Anahtar Kelimeler: Girişim Filtreleri, Optik Kaplama, İnce Film, Kaplama Teknikleri, Fiziksel Buharlaştıma Yöntemi, CCD, Geçirgenlik, Yansıma, OptiLayer

To my mom and dad...

ACKNOWLEDGMENTS

It would not have been possible to write this thesis without the help and support of the kind people around me, to only some of whom it is possible to give particular mention here.

I would like to express my sincere gratitude to my advisor Assoc. Prof. Dr. Akif Esendemir for the help of my study and research, for his patience, motivation, and immense knowledge.

I would like to thank to my friends and colleagues Esra Benli Öztürk and Vural Köksal for their continuous support.

I also would like to thank to my family for their love and support throughout my life. I am really lucky person to have such a perfect family.

Finally, I wish to give special thanks to my best friend Sinem Taşbilek, to Oğuzhan Öztürk and to Fatime Zehra Adil for their personal support and great patience at all times.

TABLE OF CONTENTS

ABSTRACT iv

ÖZ v

ACKNOWLEDGMENTS vii

TABLE OF CONTENTS viii

LIST OF TABLES xi

LIST OF FIGURES xii

CHAPTERS

1 INTRODUCTION 1

1.1 Introduction 1

1.2 Image Sensors 3

1.2.1 Charge-Coupled Devices (CCDs) 4

1.2.2 Kodak KLI-4104 Image Sensor 6

1.3 The Content Of The Study 9

2 BASICS OF COATING 10

2.1 Thin Film 10

2.2 Basic Theory 11

2.2.1 Reflectance and Transmittance at Normal Incidence 18

2.3 Optical Coatings 19

2.3.1 Antireflective Coatings 19

2.3.1.1 Single Layer Antireflective Coating 19

2.3.1.2 Multi-Layer Antireflective Coating 19

2.3.2 High-Reflective Coatings 21

2.3.3 Edge Filters 22

3 THIN FILM PRODUCTION 23
3.1 Thin Film Processing 23
3.2 Thin-Film Deposition Techniques 25
3.2.1 Chemical Vapor Deposition 25
3.2.2 Physical Vapor Deposition 27
3.2.2.1 Sputtering 28
3.2.2.2 Evaporation 29
4 THE COATING SYSTEM 32
4.1 System Overview 32
4.2 The Vacuum Chamber 33
4.2.1 Electron Beam (e-beam) Evaporation Source 35
4.2.2 Advanced Plasma Source (APS) 36
4.2.3 Thickness Measurement Systems 38
4.2.3.1 Quartz Crystal Measurement System (XMS) . 39
4.2.3.2 Optical Monitoring System (OMS) 39
4.2.3.3 Tooling Factor 43
5 DESIGN AND PRODUCTION OF THE FILTERS 45
5.1 The Material Selection 45
5.1.1 Silicon Dioxide (SiO_2) 45
5.1.2 Titanium Dioxide (TiO_2) 46
5.2 Tooling Factors and Wavelength-Dependent Refractive Indices . . . 46
5.3 Design of the Optical Filters 52
5.3.1 The Design Program: OptiLayer Thin Film Software . . . 52
Refinement 53
Needle Optimization 53
Gradual Evolution 53
5.3.2 The Design Procedure 55
5.3.2.1 Design of Short-Pass Filter 56
5.3.2.2 Design of Long-Pass Filter 59
5.4 Production of Filters 64

5.4.1 The Coating Process 64
5.4.2 Spectroscopic Measurements 66
5.4.2.1 The Spectrophotometer: Perkin Elmer - Lambda 950 66
5.4.2.2 The Measurement Results 68
6 CONCLUSION 71
REFERENCES 75
APPENDICES
A WAVELENGTH-DEPENDENT REFRACTIVE INDEX of B270 77

LIST OF TABLES

TABLES

Table 1.1 General features of Kodak KLI-4104 sensor 6

Table 1.2 The specifications of required filters 8

Table 3.1 Special features for typical coating processes 31

Table 5.1 The general features of SiO_2 46

Table 5.2 The general features of TiO_2 46

Table 6.1 Specifications of produced optical filters 72

Table A.1 Dispersion Data of B270 Glass (obtained from manufacturer) 77

LIST OF FIGURES

FIGURES

Figure 1.1 Basic parts of a CCD 4

Figure 1.2 CCD readout steps 5

Figure 1.3 Block diagram of KLI-4104 CCD sensor 7

Figure 1.4 KLI-4104 Image Sensor typical responsivity 7

Figure 1.5 Cut-off values for short-pass and long-pass filters 8

Figure 2.1 The behavior of light on the surface of thin film coated substrate 10

Figure 2.2 The electromagnetic fields at the thin film boundaries when $\vec{E}$ is perpendicular to the plane of incidence 12

Figure 2.3 The electromagnetic fields at the thin film boundaries when $\vec{E}$ is parallel to the plane of incidence 15

Figure 2.4 High reflectance stack 21

Figure 3.1 Cross-section views of the early stages of film growth 24

Figure 3.2 Conventional chemical vapor deposition process 27

Figure 3.3 Basic scheme of sputtering process 29

Figure 3.4 Evaporation methods 30

Figure 4.1 Vacuum chamber 33

Figure 4.2 The schematic representation of the e-beam evaporation source 35

Figure 4.3 Operation principle of the plasma ion-assisted deposition and cross section of the APS 37

Figure 4.4 Combined measuring head 39

Figure 4.5 Reflections from coated test slide 40

Figure 4.6 Thickness-dependent curves obtained by OMS 41
Figure 4.7 Favorable areas for cut-off point 42
Figure 4.8 Basic structure of OMS 42

Figure 5.1 Reflection curve of single layer SiO_2 coating 49
Figure 5.2 Transmission curve of single layer TiO_2 50
Figure 5.3 Wavelength-dependent refractive index of SiO_2 51
Figure 5.4 Wavelength-dependent refractive index of TiO_2 51
Figure 5.5 Extinction coefficients of SiO_2 and TiO_2 52
Figure 5.6 The gradual evolution window 54
Figure 5.7 Description of coating materials 55
Figure 5.8 Definition of the target 56
Figure 5.9 9-layer initial design for short-pass filter 57
Figure 5.10 24-layer design for narrow target 57
Figure 5.11 32-layer design for short-pass filter 58
Figure 5.12 Backside effect 58
Figure 5.13 Final design for short-pass filter 59
Figure 5.14 13-layer initial design for long-pass filter 60
Figure 5.15 13-layer initial design after refinement 60
Figure 5.16 32-layer design for narrow target 61
Figure 5.17 64-layer design 62
Figure 5.18 37-layer design for long-pass filter 62
Figure 5.19 Effect of backside reflection 63
Figure 5.20 Final design for long-pass filter 63
Figure 5.21 Filter glasses 64
Figure 5.22 Holder for filter glasses 64
Figure 5.23 Monitoring for short-pass filter 65
Figure 5.24 Monitoring for long-pass filter 66
Figure 5.25 Schematic diagram of the optical system in spectrophotometer. 67

Figure 5.26 Single side coated short-pass filter 68

Figure 5.27 Short-pass filter with backside coating 69

Figure 5.28 Single side coated long-pass filter 69

Figure 5.29 Long-pass filter with backside coating 70

Figure 6.1 Responsivity curve of CCD with short-pass filter. 73

Figure 6.2 Resposivity curve of CCD with long-pass filter. 73

CHAPTER 1

INTRODUCTION

1.1 Introduction

Thin film technology has many applications in everyday life. With developing technology, thin film phenomena have become an important issue in different areas. In optical applications, the reflection and the transmission properties of optical components can be altered by applying thin film coatings on their surfaces. A specific range of coming light beam can be totally eliminated or the intensity of the range can be decreased by optical coatings. The physics behind the thin film coatings is interference.

The scientific history of the thin film phenomena is based on 17th century. The earliest descriptions of the thin film were published by J. M. Marci (1648), R. Boyle (1663), F. M. Grimaldi (1665) and R. Hooke (1665) who tried to find explanation for colored reflection from soap bubbles, from air wedges between glass surfaces and from the oil slicks. However, these publications were not enough to explain these phenomena and they only included some ideas in terms of reflection and refraction. The works of Isaac Newton (1704) on the nature of light cause a big advance in understanding these colors but the complete explanation could be done after the works of Young and Fresnel in the 19th century. It was discovered that the reason of the colors is interference of light waves [1]. The following contributors were Huygen, Poisson, Airy, Stoke, Maxwell, Fabry Perot, Fraunhofer, Rayleigh, Taylor and the foundation of physical optics laid by these scientists and others was of the essence for the design of optical coatings. However, for the production of optical coatings, the improvements in technology were needed.

In the 1930s, with the adequate advances in vacuum technology, the production of the modern

thin film coatings has become possible. Since then, the level of sophistication and the quality of the coatings have improved with the development in vacuum and deposition technology.

Today, it is possible to design and product high-quality thin film coatings on the surface of any optical element to achieve the desired transmission - reflection ratio by using the interference property of light. Basically, the principle is that if two light waves coming from the surfaces of two parallel plates are in phase, they constructively interfere. This means that the optical path difference between these two waves is an exact multiple of the wavelength. With the same logic, if the optical path difference between these two light waves is one-half wavelength or odd multiple of it then they will be out of phase and they destructively interfere. Optical coatings can consist of one to hundreds of thin layers [2]. By changing the material type and the thickness of each layer, it is possible to determine the amplitude and the phase of reflected or transmitted light at each interface and control transmittance or reflectance of the coating as a function of wavelength.

In applications, the requirement is that the reflected part of incident light approaches zero for lenses (anti-reflective coating); 100% for mirrors (reflective coatings); a fixed intermediate value for beamsplitters. Or, the reflected portion of the light approaches zero for some wavelengths while it approaches 100% for the others for optical filters. Each has different application areas. For instance, the lenses and prisms used in cameras, binoculars, telescopes, and microscopes are coated to give anti-reflective (AR) properties since, generally, 4-5 percent of incident light reflects from each surface of uncoated optical glasses and, for tools including more than one component, the loss in transmitted light become important. Also, the screens of mobile phones and other mobile devices, the surface of aircraft instrumentation panels are antireflective coated to improve the visibility of the displays.

Reflective coatings are used in scanners, astronomy telescopes, photocopy machines, manufacture of compact disks etc. Also, in the laser systems, in order to direct the laser to the target, mirrors are used.

Just as electrical filters block certain frequencies, optical filters absorb or reflect certain wavelengths and allow the desired range of wavelength to pass through. Optical filters are used in digital cameras to filter infrared light which affects the image quality and to conserve the imaging sensor. Also, there are optical filters in front projection displays to cut off the harmful ultraviolet and infrared light but not the visible. Narrowband optical filters are also used in op-

tical telecommunication systems to separate the light into different wavelength components. Also, some special filters are used for specific applications. For example, a filter, called cold mirror, is used in lighting system of operating theatres because while it reflects the visible light, it transmits the infrared in other words it transmits the heat [3].

In the present work, it is aimed to design and produce two different optical edge filters to be able to obtain image in two bands, visible and near-infrared, with two, identical CCD sensors. These sensors are used in imaging system of a satellite and have spectral responsivity between 350 - 1050 nm. To define the specifications of the necessary filters, the general properties of CCD used should be known. Therefore, the general information about CCDs and the properties of the selected CCD are given below.

1.2 Image Sensors

In the capture of an image by a camera, light passes through a system composed of lens-mirror combination and falls on an image sensor. Presently, there are two important technologies that can be used to capture images in a camera, i.e. CCD (Charge-Coupled Device) or CMOS (Complementary Metal-Oxide Semiconductor). An image sensor consists of individual detector elements called pixels that convert the incoming light into a corresponding amount of electrons. After conversion of these electrons into voltage and transformation of them into numbers by converters, a signal is constituted. Image sensors register the light without any color information. Therefore, for color imaging, the optical spectrum of incident image should be separated into 3 color bands. This color separation is accomplished by color filters (typically deposited organic dyes), that may act as transmission or absorbing filters, on the imager surface. The most common color registration method is RGB (Red, Green, Blue) because they are primary colors that can generate all visible colors with different combination. In such a sensor, there are three channels which are covered with red, green and blue bandpass filter individually so that all color information of an image can be obtained by one single scan.

In the astronomical applications, generally charge-coupled devices (CCDs) are used as image sensors.

1.2.1 Charge-Coupled Devices (CCDs)

A CCD is a device composed of an array of capacitors (one capacitor per pixel) equipped with circuitry to read out the stored charge after an exposure time [4]. To understand the operation of a CCD, lets suppose a telescope with a matrix of capacitors at its focal plane. In the exposure time, incoming light excites the electrons, in other words; photoelectrons are formed by photoelectric effect and they accumulate at the pixels that are subjected to illumination. Note that before the exposure time all capacitor wells should be empty. The number of accumulated photoelectrons is proportional to the rate of photon coming on the pixel. Figure 1.1 shows the major parts of the sensor. Dots correspond to the stored electrons at the end of the exposure.

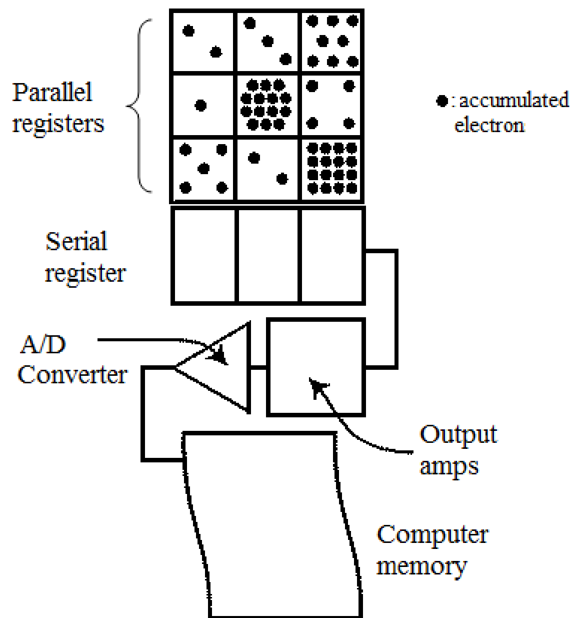

Figure 1.1: Basic parts of a CCD

In this case, the light sensitive matrix of capacitors has three rows and three columns. As shown in the figure, the column of pixels in this matrix is called parallel register and the additional row located at the lower edge of the matrix is called serial register. As the parallel registers comprise the entire light sensitive array, the serial register is preserved from the light.

The serial register consist one pixel for each parallel registers column. The steps of reading the array are shown in the Figure 1.2.

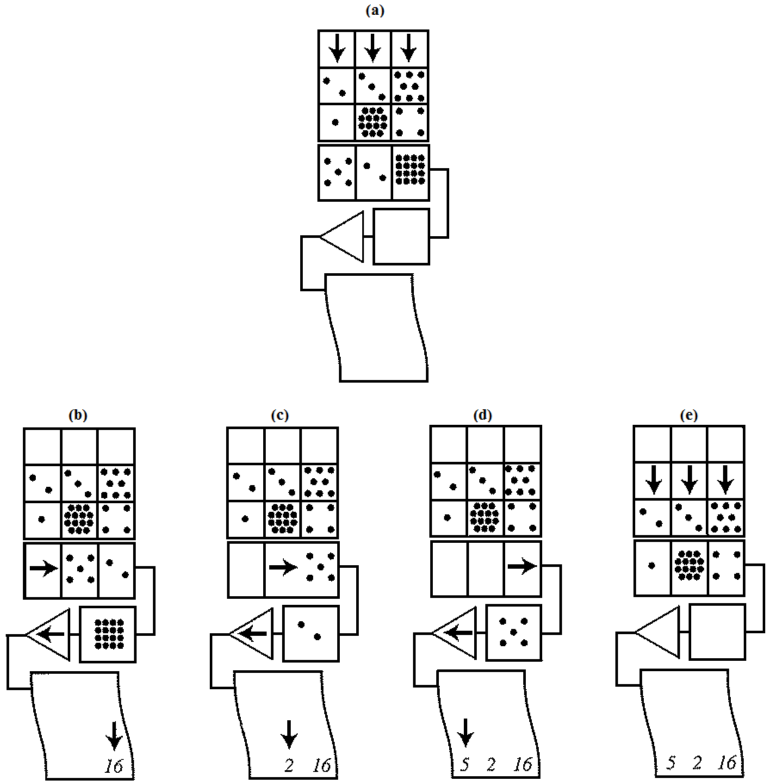

Figure 1.2: CCD readout steps

Pixel-by-pixel shifting is the main issue in the processing of the stored data. First, data in the parallel registers is shifted down the columns by one pixel so that, in this case, electrons stored 3rd row of the parallel registers move to the serial register, electrons in the 2nd row shift to 3rd row and electrons in the 1st row shift to the 2nd one as shown in the Figure 1.2 (a). Then, electrons in the serial register shift to the right by one pixel and the electrons in the rightmost pixel move into output amplifier as shown in the Figure 1.2 (b). The conversion of the charge into a voltage takes place in the output amplifier. The next place that the data move to is analog to digital (A/D) converter . A/D converter converts the voltage to a binary number and this number is stored in a computer memory (Figure 1.2(c)). This shift in the serial register continues until the electrons in all serial register pixels have been processed (Figure 1.2(d)). Then, the whole operation steps repeat for the next parallel register row (Figure 1.2(e)). The

process ends when the entire array has been read and saved at the memory.

In our case, Kodak KLI-4104 image sensor is used in the electronic unit of the space camera.

1.2.2 Kodak KLI-4104 Image Sensor

The Kodak KLI-4104 is a multi spectral, linear, solid state image sensor. It contains three parallel photodiode arrays of 4080 active photo-elements. One array is covered with red filter (red channel), second array is covered with green filter (green channel) and the last is covered with blue filter (blue channel). The sensor also has a fourth channel with 8160 active photo-elements that has a monochrome response (luminance channel). The height and pitch of the pixels is 10 micron for R, G, B channels and 5 micron for the luminance channel. Each channel has a number of pixels at the beginning and at the end of the array for dark reference and test. Basic features of the sensor and block diagram are shown in the Table 1A and Figure 1.3, respectively.

Table 1.1: General features of Kodak KLI-4104 sensor

Parameter	**Value**
Total Number of Pixels	3×4134 Chroma, 1×8292 Luma
Number of Effective Pixels	3×4128 Chroma, 1×8276 Luma
Number of Active Pixels	3×4080 Chroma, 1×8160 Luma
Pixel Size	10 µm (H) × 10 µm (V) Chroma, 5 µm (H) × 5 µm (V) Luma,
Pixel Pitch	10 µm Chroma, 5 µm Luma,
Inter-Array Spacing, G to R, R to B B to L	90 µm (9 lines effective) 122.5 µm (12.25 lines effective)
Quantum Efficiency	62%(B), 62%(G), 80%(R), 85%(L)
Output Sensitivity	Chroma - 14 µV/electron Luma - 11 µV/electron
Responsivity [R/G/B/L]	17(B), 20(G), 32(R), 27(L) V/µJ/cm^2
Total Read Noise	120 electrons
Dark Current	Chroma 0.007 pA/pixel Luma 0.0008 pA/pixel

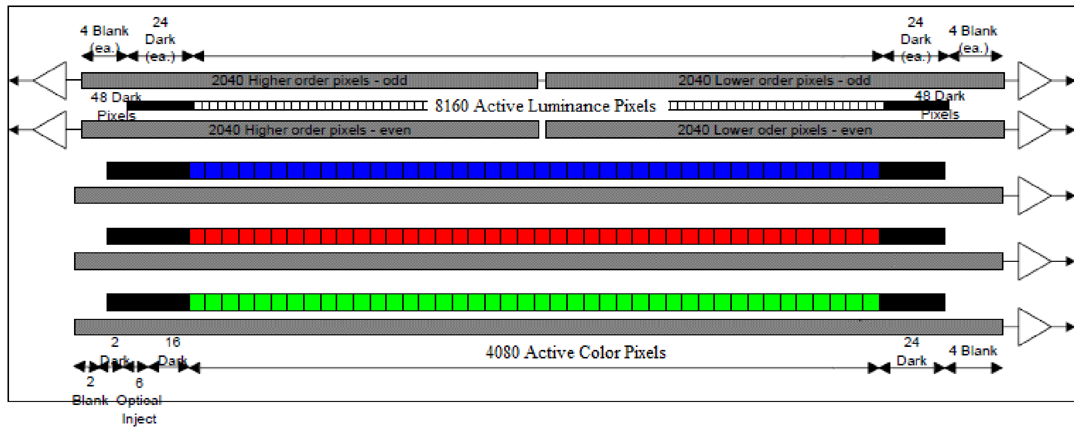

Figure 1.3: Block diagram of KLI-4104 CCD sensor

The responsivity of the image sensor is shown in the Figure 1.4.

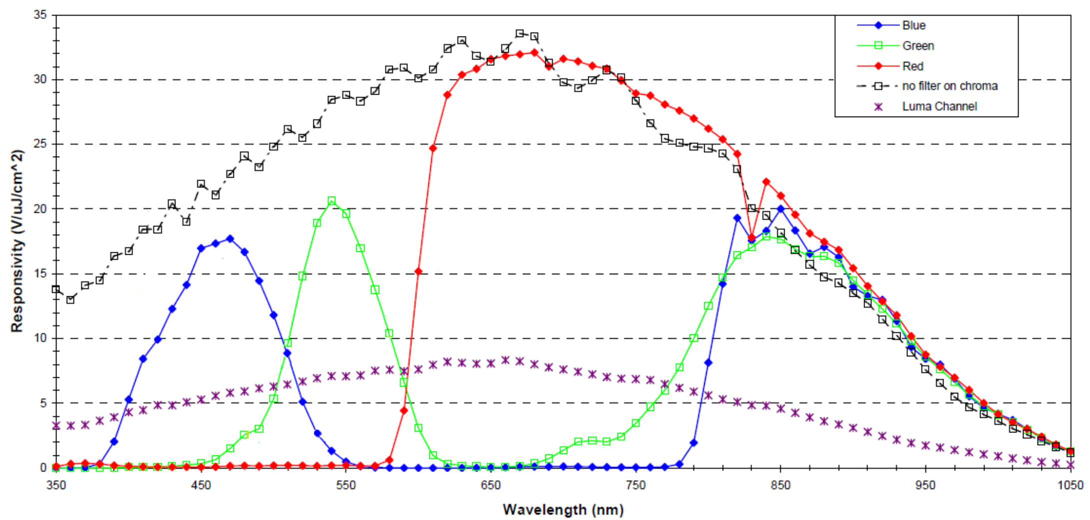

Figure 1.4: KLI-4104 Image Sensor typical responsivity

As shown in the Figure 1.4, beyond the 750 nm, all channels display high transmission which means the filters on them become transparent. Therefore, obtaining an image in the near-infrared (NIR) by this image sensor is also possible. While pure image in the visible spectrum can be obtained by using a filter that transmits the smaller wavelength and reflects beyond the 700nm, NIR image can be obtained with the same CCD by using another filter that transmits

beyond the 750 nm and reflects others. Figure 1.5 shows the cut off values for RGB filter (short-pass filter) and NIR filter (long-pass filter) on the responsivity graph of the KLI-4104 image sensor.

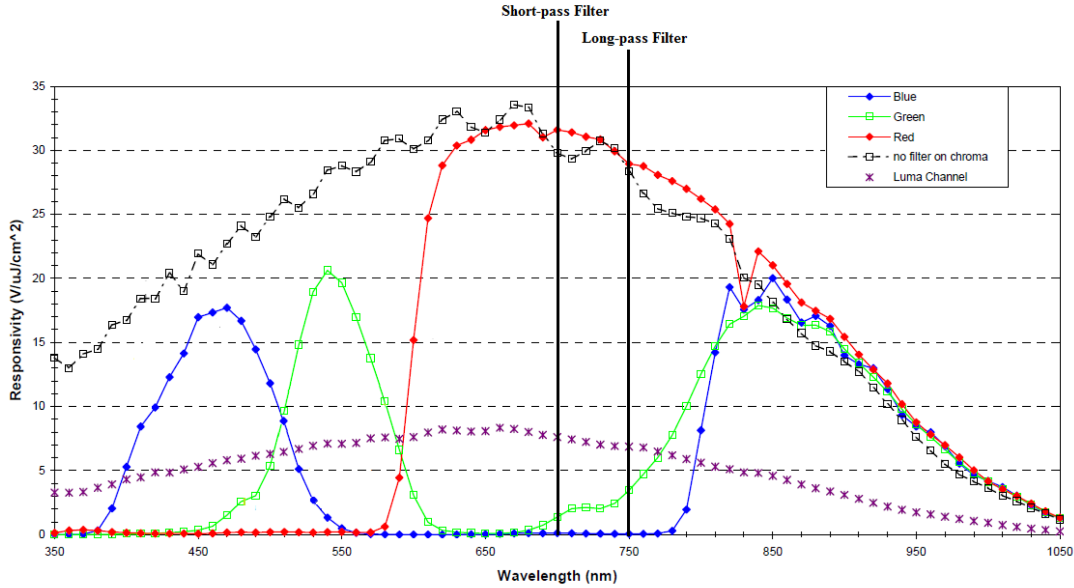

Figure 1.5: Cut-off values for short-pass and long-pass filters

As the wavelength range getting larger, the design of the filters gets harder. Therefore, the wavelength range can be bounded between 370 – 1050 nm since the responsivity of CCD beyond this range is negligible. Briefly, the requirements for the filters are given below.

Table 1.2: The specifications of required filters

The Requirements	Wavelength Range	Cut-off Wavelength	Transmission Zone (>90%)	Reflection Zone (>95%)
Short-pass Filter	370 – 1000 nm	700 nm	370 – 700 nm	700 – 1000 nm
Long-pass Filter	370 – 1000 nm	750 nm	750 – 1000 nm	370 – 750 nm

1.3 The Content Of The Study

In the present work, it is aimed to produce one short-pass and one long-pass edge filter for CCD surfaces in order to obtain pure RGB and pure NIR images as mentioned in previous subsections. The design and optimization are also the main items of this work. For this purpose, a brief information about the image sensors and the working principle of CCDs are given, the general properties of CCD KLI-4104 are mentioned and the problem is indentified in the introduction part.

In chapter 2, basic principles of coatings are studied. The basic theory of the thin film is explained and antireflective coating, high reflective coating and edge filters are examined.

In chapter 3, the stages of thin film production and the factors affecting the film properties are discussed. Also, thin film deposition techniques with their advantages and disadvantages are studied.

In chapter 4, the coating system used in the production of filters is presented and the most important parts; e-beam source, advanced plasma source and thickness measurement systems are explained in detail.

In chapter 5, all experimental work performed to design and produce the filters is presented. The tools and equipments used in design and measurements are introduced briefly. Also, the results of measurement are given at the end of this chapter.

Finally, the summary of all work with discussions and conclusion is presented in chapter 6.

CHAPTER 2

BASICS OF COATING

2.1 Thin Film

Thin film is generally defined as the layer whose thickness is less than 1 micrometer. Thin films are produced by evaporating of selected materials on an appropriate substrate. The behavior of the incoming light on the surface of thin film-coated substrate is shown in the Figure 2.1.

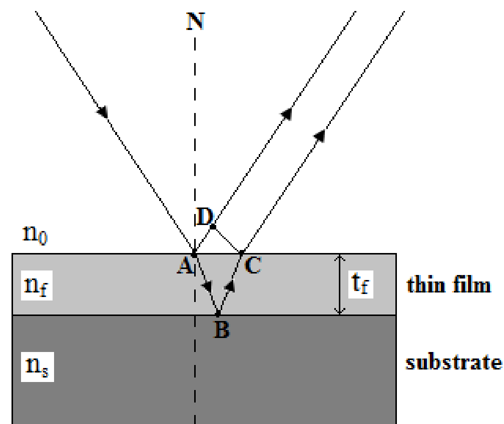

Figure 2.1: The behavior of light on the surface of thin film coated substrate

Optical interference filters use the interference property of light. The path difference caused by the thin film generates a phase difference in reflected beams. According to the figure, the optical path difference, $\triangle$, can be defined as

$$\triangle = (\overline{AB} + \overline{BC})n_f - \overline{AD}n_o \tag{2.1}$$

Where n_f and n_o are the refractive indices of the thin film and the medium, respectively. By using geometric and trigonometric relations for $\overline{AB}$, $\overline{BC}$ and $\overline{AD}$, the path difference can be found as

$$\triangle = 2n_f t_f cos\alpha \tag{2.2}$$

where α is the angle between the $\overline{AB}$ and the normal. Since the phase difference is equal to wave number ($k = 2\pi/\lambda$) times $\triangle$, we can say that if the path difference is equal to the wavelength of the incoming light then the reflected beams will be in phase and so the constructive interference will occur. If $\triangle = \lambda/2$ then the phase shift will be π and so the reflected beams will be out of phase. In this case, the destructive interference will occur. Here, for simplicity, only two reflections are taken into account, but in reality multiple reflections take place.

In brief, in the design of optical interference filters, the refractive index and the thickness of the film can be altered to obtain desired reflection & transmission rates. This means that the selection of material types and deciding their thickness is important for production of the filters.

2.2 Basic Theory

Before explaining the theory of thin film, it is appropriate to give Maxwells equations.

$$\nabla.\vec{E} = \frac{\rho}{\varepsilon_o} \tag{2.3}$$

$$\nabla.\vec{B} = 0 \tag{2.4}$$

$$\nabla \times \vec{E} = -\frac{\partial \vec{B}}{\partial t} \tag{2.5}$$

$$\nabla \times \vec{B} = \mu_o \vec{J} + \mu_o \varepsilon_o \frac{\partial \vec{E}}{\partial t} \tag{2.6}$$

In vacuum, the conditions $\rho = 0$ and $J = 0$ are met.

The optical thin film theory can be explained by the electric & magnetic fields in the regions and their boundary conditions. The electric field and the magnetic field magnitudes are related by

$$E = \upsilon B \tag{2.7}$$

where the wave speed υ is

$$\upsilon = \frac{c}{n} \tag{2.8}$$

In vacuum,

$$c = \frac{1}{\sqrt{\varepsilon_o \mu_o}} \tag{2.9}$$

where ε_o is permittivity, μ_o is permeability of free space. By combining Equations (2.7), (2.8) and (2.9) , we can obtain

$$B = \frac{E}{\upsilon} = \left(\frac{n}{c}\right) E = n\sqrt{\varepsilon_o \mu_o} E \tag{2.10}$$

By using $B = \mu_o H$, it is found that

$$\sqrt{\frac{\mu_o}{\varepsilon_o}} H = nE \tag{2.11}$$

Here, $\sqrt{\frac{\mu_o}{\varepsilon_o}}$ is defined as the impedance of free space which is represented by Z_o. In Figure 2.2, the behavior of the linearly polarized light coming on a thin film-substrate combination is shown. n_o, n_f, n_s are the refractive indices of the incident medium, thin film and substrate, respectively. Assume that the thin film layer is nonabsorbing, isotropic, homogeneous and uniform in thickness and $\vec{E}$ is pointing out of the page.

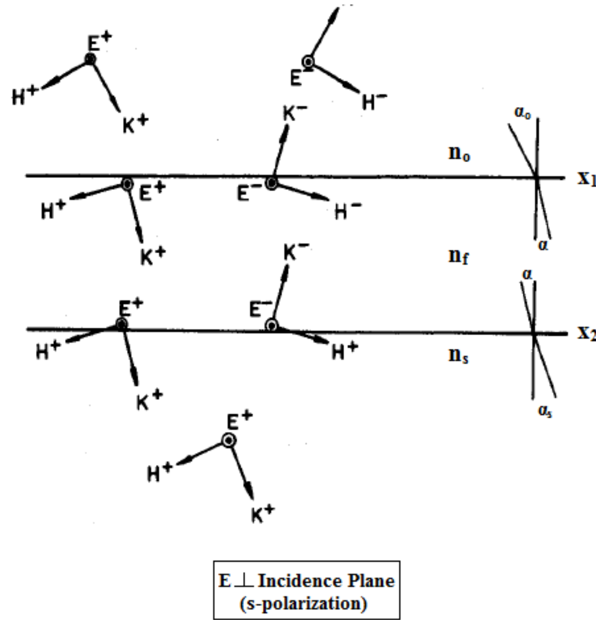

Figure 2.2: The electromagnetic fields at the thin film boundaries when $\vec{E}$ is perpendicular to the plane of incidence [5]

According to the Figure 2.2, the notations of E^{+}, H^{+}, K^{+} belong to the positive-going waves which is in the direction of incident light and E^{-}, H^{-}, K^{-} are belong to negative ones. We have two boundaries that are $x = x_1$ for incident medium-thin film interface and $x = x_2$ for thin film-substrate interface. The notations $x - \delta$ and $x + \delta$ are used to describe the two sides at the boundaries.

Boundary conditions following from Maxwell's equations require continuity of the tangential components of both electric $\vec{E}$ and magnetic $\vec{H}$ field vectors across the interfaces x_1 and x_2. This means that the magnitudes of the fields are equal on both sides. So, at boundary $x = x_1$,

$$\begin{aligned} E(x_1) &= E^{+}(x_1 - \delta) + E^{-}(x_1 - \delta) \\ &= E^{+}(x_1 + \delta) + E^{-}(x_1 + \delta) \end{aligned} \tag{2.12}$$

$$\begin{aligned} H(x_1) &= H^{+}(x_1 - \delta) cos\alpha_o - H^{-}(x_1 - \delta) cos\alpha_o \\ &= H^{+}(x_1 + \delta) cos\alpha - H^{-}(x_1 + \delta) cos\alpha \end{aligned} \tag{2.13}$$

By using Equation (2.11),

$$\begin{aligned} Z_o H(x_1) &= [E^{+}(x_1 - \delta) - E^{-}(x_1 - \delta)] n_o cos\alpha_o \\ &= [E^{+}(x_1 + \delta) - E^{-}(x_1 + \delta)] n_f cos\alpha \end{aligned} \tag{2.14}$$

where α_o is the angle of incidence and α is the angle specified from Snells law $n_o sin\alpha_o = n_f sin\alpha$. At boundary $x = x_2$,

$$\begin{aligned} E(x_2) &= E^{+}(x_2 - \delta) + E^{-}(x_2 - \delta) \\ &= E^{+}(x_2 + \delta) \end{aligned} \tag{2.15}$$

$$\begin{aligned} H(x_2) &= H^{+}(x_2 - \delta) cos\alpha - H^{-}(x_2 - \delta) cos\alpha \\ &= H^{+}(x_2 + \delta) cos\alpha_s \end{aligned} \tag{2.16}$$

and so

$$\begin{aligned} Z_o H(x_2) &= [E^{+}(x_2 - \delta) - E^{-}(x_2 - \delta)] n_f cos\alpha \\ &= E^{+}(x_2 + \delta) n_s cos\alpha_s \end{aligned} \tag{2.17}$$

where α_s again is determined from Snells law ($n_f sin\alpha = n_s sin\alpha_s$). A phase shift is observed as the wave traverses the thin film layer. Equation (2.2) found in Section 2.1 represents the

optical path length in the film so the optical path length related with only one traversal is $\triangle_1 = \frac{\triangle}{2} = n_f t cos\alpha$ and the phase shift

$$\varnothing = k\triangle_1 = \frac{2\pi}{\lambda} n_f t_f cos\alpha \tag{2.18}$$

where the physical thickness t_f can be written as $x_2 - x_1$. Thus,

$$E^+(x_2 - \delta) = E^+(x_1 + \delta)e^{i\varnothing} \tag{2.19a}$$

$$E^-(x_2 - \delta) = E^-(x_1 + \delta)e^{i\varnothing}. \tag{2.19b}$$

So we can rewrite Equations (2.15) and (2.17) as

$$E(x_2) = E^+(x_1 + \delta)e^{-i\varnothing} + E^-(x_1 + \delta)e^{i\varnothing} \tag{2.20}$$

$$Z_o H(x_2) = [E^+(x_1 + \delta)e^{-i\varnothing} - E^-(x_1 + \delta)e^{i\varnothing}]n_f cos\alpha \tag{2.21}$$

When we solve these two equations for $E^+(x_1 + \delta)$ and $E^-(x_1 + \delta)$, we can find

$$E^+(x_1 + \delta) = \frac{1}{2}\left[E(x_2) + \frac{Z_o H(x_2)}{n_f cos\alpha}\right]e^{i\varnothing} \tag{2.22}$$

$$E^-(x_1 + \delta) = \frac{1}{2}\left[E(x_2) - \frac{Z_o H(x_2)}{n_f cos\alpha}\right]e^{-i\varnothing} \tag{2.23}$$

By substituting these into Equarion (2.12) & (2.14) and using the Euler identities;

$$cos\varnothing = \frac{e^{i\varnothing} + e^{-i\varnothing}}{2} \quad \& \quad isin\varnothing = \frac{e^{i\varnothing} - e^{-i\varnothing}}{2}, \tag{2.24}$$

we obtain

$$E(x_1) = E(x_2)cos\varnothing + i\frac{Z_o H(x_2)}{n_f cos\alpha} sin\varnothing \tag{2.25}$$

and

$$Z_o H(x_1) = E(x_2)i(n_f cos\alpha)sin\varnothing + Z_o H(x_2)cos\varnothing. \tag{2.26}$$

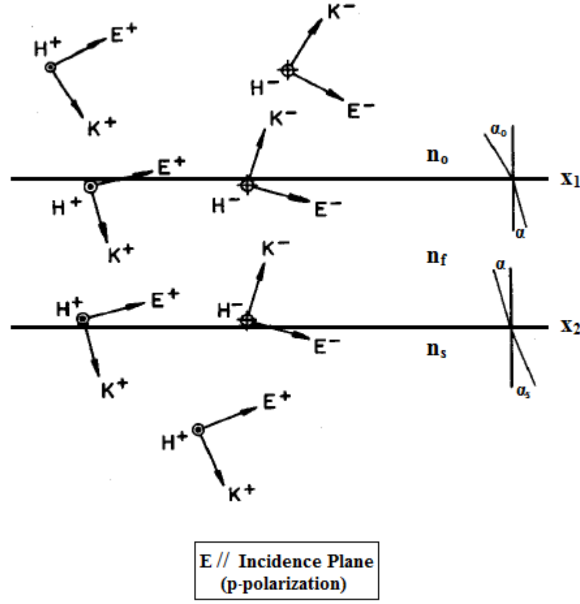

Figure 2.3: The electromagnetic fields at the thin film boundaries when $\vec{E}$ is parallel to the plane of incidence [5]

If $\vec{E}$ is parallel to the incidence plane (p-polarization) as shown in the Figure 2.3, the equations for boundary $x = x_1$ becomes

$$\begin{aligned} E(x_1) &= [E^+(x_1 - \delta) + E^-(x_1 - \delta)]cos\alpha_o \\ &= [E^+(x_1 + \delta) + E^-(x_1 + \delta)]cos\alpha \end{aligned} \tag{2.27}$$

$$\begin{aligned} Z_oH(x_1) &= [E^+(x_1 - \delta) - E^-(x_1 - \delta)]n_o \\ &= [E^+(x_1 + \delta) - E^-(x_1 + \delta)]n_f \end{aligned} \tag{2.28}$$

and for boundary $x = x_2$ becomes

$$\begin{aligned} E(x_2) &= [E^+(x_2 - \delta) + E^-(x_2 - \delta)]cos\alpha_o \\ &= [E^+(x_1 + \delta)e{-}i\varnothing + E^-(x_1 + \delta)e^{i\varnothing}]cos\alpha \end{aligned} \tag{2.29}$$

$$\begin{aligned} Z_oH(x_2) &= [E^+(x_2 - \delta) - E^-(x_2 - \delta)]n_f \\ &= [E^+(x_1 + \delta)e^{-i\varnothing} - E^-(x_1 + \delta)e^{i\varnothing}]n_f \end{aligned} \tag{2.30}$$

Similarly as in the s-polarization case, we can find

$$E(x_1) = E(x_2)cos\varnothing + i\,\frac{Z_oH(x_2)}{n_f/cos\alpha}sin\varnothing \tag{2.31}$$

and

$$Z_oH(x_1) = E(x_2)i(n_f/cos\alpha)sin\varnothing + Z_oH(x_2)cos\varnothing. \tag{2.32}$$

It is apparent that by putting $n_f/cos\alpha$ instead of $n_f cos\alpha$ in the resultant equations in s-polarization case, one can obtain the equations for p-polarization case. Therefore, we can reduce these four equations into two as

$$E(x_1) = E(x_2)cos\varnothing + i\frac{Z_oH(x_2)}{n}sin\varnothing \tag{2.33}$$

and

$$Z_oH(x_1) = E(x_2)insin\varnothing + Z_oH(x_2)cos\varnothing. \tag{2.34}$$

where

$$n = \begin{cases} n_f cos\alpha & \text{for s-polarization} \\ n_f/cos\alpha & \text{for p-polarization} \\ n_f & \text{for normal light incidence} \end{cases}$$

The Equations (2.33) and (2.34) can be written in matrix form as

$$\begin{pmatrix} E(x_1) \\ Z_oH(x_1) \end{pmatrix} = \begin{pmatrix} cos\varnothing & i\,\frac{sin\varnothing}{n} \\ insin\varnothing & cos\varnothing \end{pmatrix} \begin{pmatrix} E(x_2) \\ Z_oH(x_2) \end{pmatrix} \tag{2.35}$$

The $2x2$ matrix is named “characteristic matrix” of the single thin film and generally represented by

$$M = \begin{pmatrix} m_{11} & m_{12} \\ m_{21} & m_{22} \end{pmatrix} \tag{2.36}$$

If x_2 would be the interface between two different thin film layers; then, we would have three boundaries ($x = x_1$, $x = x_2$ and $x = x_3$). Then the relations between the fields $E(x_2)$ & $H(x_2)$ and the fields $E(x_3)$ & $H(x_3)$ would be provided by a second characteristic matrix as

$$\begin{pmatrix} E(x_2) \\ Z_oH(x_2) \end{pmatrix} = M_2 \begin{pmatrix} E(x_3) \\ Z_oH(x_3) \end{pmatrix} \tag{2.37}$$

If we multiply both sides with M_1, we can obtain

$$\begin{pmatrix} E(x_1) \\ Z_oH(x_1) \end{pmatrix} = M_1M_2 \begin{pmatrix} E(x_3) \\ Z_oH(x_3) \end{pmatrix} \tag{2.38}$$

When we generalize the result for N-layer coating, we have

$$\begin{pmatrix} E(x_1) \\ Z_oH(x_1) \end{pmatrix} = M_1M_2...M_N \begin{pmatrix} E(x_{N+1}) \\ Z_oH(x_{N+1}) \end{pmatrix} \tag{2.39}$$

As seen above, the characteristic matrix of multilayer thin films is obtained by multiplying individual characteristic matrices

$$M = M_1 M_2 ... M_N$$

Now, if we reconsider the Equations (2.12), (2.14), (2.15) and (2.17)

$$E(x_1) = E^+(x_1 - \delta) + E^-(x_1 - \delta)$$

$$E(x_2) = E^+(x_2 + \delta)$$

$$Z_o H(x_1) = [E^+(x_1 - \delta) - E^-(x_1 - \delta)] n_o cos\alpha_o$$

$$Z_o H(x_2) = E^+(x_2 + \delta) n_s cos\alpha_s$$

The Equation (2.35) becomes

$$\begin{pmatrix} E^+(x_1 - \delta) + E^-(x_1 - \delta) \\ (E^+(x_1 - \delta) - E^-(x_1 - \delta)) n_o cos\alpha_o \end{pmatrix} = \begin{pmatrix} cos\varnothing & i\,\frac{sin\varnothing}{n} \\ insin\varnothing & cos\varnothing \end{pmatrix} \begin{pmatrix} E^+(x_2 + \delta) \\ E^+(x_2 + \delta) n_s cos\alpha_s \end{pmatrix}$$
$$= \begin{pmatrix} m_{11} & m_{12} \\ m_{21} & m_{22} \end{pmatrix} \begin{pmatrix} E^+(x_2 + \delta) \\ E^+(x_2 + \delta) n_s cos\alpha_s \end{pmatrix} \quad (2.40)$$

This matrix form leads to two equations:

$$E^+(x_1 - \delta) + E^-(x_1 - \delta) = m_{11} E^+(x_2 + \delta) + m_{12} E^+(x_2 + \delta) n_s cos\alpha_s \quad (2.41)$$

$$[E^+(x_1 - \delta) - E^-(x_1 - \delta)] n_o cos\alpha_o = m_{21} E^+(x_2 + \delta) + m_{22} E^+(x_2 + \delta) n_s cos\alpha_s \quad (2.42)$$

If we divide these two equations by $E^+(x_1 - \delta)$, we obtain

$$1 + \frac{E^-(x_1 - \delta}{E^+(x_1 - \delta)} = m_{11} \frac{E^+(x_2 + \delta)}{E^+(x_1 - \delta)} + m_{12} \frac{E^+(x_2 + \delta)}{E^+(x_1 - \delta)} n_s cos\alpha_s \quad (2.43)$$

$$\left(1 - \frac{E^-(x_1 - \delta}{E^+(x_1 - \delta)}\right) n_o cos\alpha_o = m_{21} \frac{E^+(x_2 + \delta)}{E^+(x_1 - \delta)} + m_{22} \frac{E^+(x_2 + \delta)}{E^+(x_1 - \delta)} n_s cos\alpha_s \quad (2.44)$$

Here, by using the definitions of reflection coefficient r & transmission coefficient t,

$$r \equiv \frac{E^-(x_1 - \delta)}{E^+(x_1 - \delta)} \quad \& \quad t \equiv \frac{E^+(x_2 + \delta)}{E^+(x_1 - \delta)}$$

we find

$$1 + r = m_{11} t + m_{12} n_s cos\alpha_s t \quad (2.45)$$

$$(1 - r) n_o cos\alpha_o = m_{21} t + m_{22} n_s cos\alpha_s t. \quad (2.46)$$

When we solve these two equations, we can obtain reflection and transmission coefficients in terms of the characteristic matrix elements as

$$r = \frac{\gamma_o m_{11} + \gamma_o \gamma_s m_{12} - m_{21} - \gamma_s m_{22}}{\gamma_o m_{11} + \gamma_o \gamma_s m_{12} + m_{21} + \gamma_s m_{22}} \quad (2.47)$$

$$t = \frac{2\gamma_o}{\gamma_o m_{11} + \gamma_o \gamma_s m_{12} + m_{21} + \gamma_s m_{22}} \quad (2.48)$$

where ,for simplicity, $n_o cos\alpha_o$ and $n_s cos\alpha_s$ are shown as γ_o and γ_s, respectively. The reflectance R and the transmittance T can be found by using r and t as

$$R = rr^* \quad (2.49)$$

and

$$T = \frac{n_s}{n_o} tt^* = 1 - R \quad (2.50)$$

Here, r^* and t^* are the complex conjugates of r and t.

2.2.1 Reflectance and Transmittance at Normal Incidence

In practice, the general case is normally or near-normal incoming light. If the light comes in the direction of normal N, all angles α_o, α and α_s are zero since the light remains perpendicular at each interface. Then, $cos\alpha_o$, $cos\alpha$ and $cos\alpha_s$ terms go to unity and so n is equal to n_f. Therefore, Equations (2.47) and (2.48) become

$$r = \frac{n_f(n_o - n_s)cos\varnothing + i(n_o n_s - n_f^2)sin\varnothing}{n_f(n_o + n_s)cos\varnothing + i(n_o n_s + n_f^2)sin\varnothing} \quad (2.51)$$

$$t = \frac{2n_o n_f}{n_f(n_o + n_s)cos\varnothing + i(n_o n_s + n_f^2)sin\varnothing} \quad (2.52)$$

According to Equation (2.51), the reflection coefficient is in the form of

$$r = \frac{A + iB}{C + iD} \quad (2.53)$$

So, reflectance for normal incidence ligth can be found by using the relation

$$rr^* = \left(\frac{A + iB}{C + iD}\right)\left(\frac{A - iB}{C - iD}\right) = \frac{A^2 + B^2}{C^2 + D^2} \quad (2.54)$$

as

$$R = \frac{n_f^2(n_o - n_s)^2 cos^2\varnothing + (n_o n_s - n_f^2)^2 sin^2\varnothing}{n_f^2(n_o + n_s)^2 cos^2\varnothing + (n_o n_s + n_f^2)^2 sin^2\varnothing}. \quad (2.55)$$

And the transmittance for normal incidence is

$$T = 1 - R = \frac{4n_f^2 n_o n_s}{n_f^2(n_o + n_s)^2 cos^2\varnothing + (n_o n_s + n_f^2)^2 sin^2\varnothing}. \quad (2.56)$$

2.3 Optical Coatings

Generally, the optical components are made of different types of glass and the surfaces of glass are coated with thin films of various materials. The main purpose is to obtain desired transmission-reflection ratio as mentioned before. With multilayer coatings, nearly zero reflection for lenses or nearly zero transmission for mirrors can be achieved in the desired wavelength range. Also, optical filters that allow the desired portion of the range pass through and reflect others can be produced.

2.3.1 Antireflective Coatings

2.3.1.1 Single Layer Antireflective Coating

According to Equation (2.2), if we want to obtain completely destructive interference in the reflected beams to have zero reflection at a wavelength, the optical thickness $n_f t_f$ should be equal to an odd number of quarter wavelengths. This means that, in accordance with Equation (2.18), the phase difference should be equal to $a(\pi/2)$ where a is an odd number so that $cos\varnothing = 0$ and $sin\varnothing = 1$. Now, Equation (2.55) becomes

$$R = \left(\frac{n_o n_s - n_f^2}{n_o n_s + n_f^2} \right)^2 . \tag{2.57}$$

Equation (2.57) shows that to make reflectance zero the refractive index of thin film material should be $\sqrt{n_o n_s}$. In brief, to have an antireflective component with single layer coating, the thin film on the surface of substrate should have index of $\sqrt{n_o n_s}$ and thickness of $\lambda/4$.

2.3.1.2 Multi-Layer Antireflective Coating

In practice, obtaining zero reflectance with single layer coating is not possible because generally the refractive index of coating materials is too high to provide the necessary condition. However, with two or more quarter-wave-thickness layers, zero reflection at a specific wavelength can be obtained. For normally incident light, since $n = n_f$ and $\varnothing = a(\pi/2)$ where a=1,3,5,... the characteristic matrix reduces to

$$M = \begin{pmatrix} 0 & \frac{i}{n_f} \\ i n_f & 0 \end{pmatrix} . \tag{2.58}$$

In two-layer case, by using the equation of characteristic matrix for multilayer coatings shown in Equation (2.2) , the characteristic matrix becomes

$$M = M_1 M_2 = \begin{pmatrix} 0 & \frac{i}{n_{f1}} \\ in_{f1} & 0 \end{pmatrix} \begin{pmatrix} 0 & \frac{i}{n_{f2}} \\ in_{f2} & 0 \end{pmatrix} = \begin{pmatrix} -\frac{n_{f2}}{n_{f1}} & 0 \\ 0 & -\frac{n_{f1}}{n_{f2}} \end{pmatrix} \quad (2.59)$$

By using new characteristic matrix elements in Equation (2.47) for normal incident light when γ_o and γ_s go to n_o and n_s respectively, we can found r as

$$r = \frac{n_o n_{f2}^2 - n_s n_{f1}^2}{n_o n_{f2}^2 + n_s n_{f1}^2}. \quad (2.60)$$

Finally, the relation between r and R shown in Equation (2.49) gives the reflectance as

$$R = \left(\frac{n_o n_{f2}^2 - n_s n_{f1}^2}{n_o n_{f2}^2 + n_s n_{f1}^2} \right)^2 . \quad (2.61)$$

According to this equation, the reflectance will be zero when $n_o n_{f2}^2 - n_s n_{f1}^2 = 0$ or

$$\frac{n_{f2}}{n_{f1}} = \sqrt{\frac{n_s}{n_o}}. \quad (2.62)$$

In the similar way, the condition for zero reflectance for three-layer case ($\lambda/4$ thickness) can be found as

$$\frac{n_{f1} n_{f3}}{n_{f2}} = \sqrt{n_o n_s}. \quad (2.63)$$

In practice, the materials having desired refractive index are not always available. Therefore, 180 ° of phase difference can be provided by optimizing the thickness of the layers produced by materials that can be obtained easily.

In the systems using polychromatic light, the absentee layers can be used to obtain broadband antireflective coatings [6]. Absentee layer is a layer having half wavelength optical thickness. The thickness of this layer is determined according to the wavelength at which the coating design is optimized (control wavelength). The total performance of the coating does not change with adding the absentee layer for this control wavelength since there would be no extra phase shift. However, this layer will have an effect on other wavelengths because the thickness chosen according to control wavelength starts to create a phase difference for other wavelengths. Therefore, by adding absentee layers, one can design multi-layer antireflective coating for a wide spectral region.

2.3.2 High-Reflective Coatings

Reflective coatings can include metallic layers like aluminum and silver or again can be composed of dielectric materials. High-reflectance dielectric coatings depend on the same principle in the dielectric antireflective coating. If we reverse the order of the layers in two-layer quarter wavelength antireflective coating in order that the incoming light meets high-index material, low-index material and substrate respectively, the reflected beams will be in phase and reflectance will increase. The structure composed of a series of such layer pairs is named a dielectric mirror or a high-reflectance stack and is schematically shown in Figure 2.4.

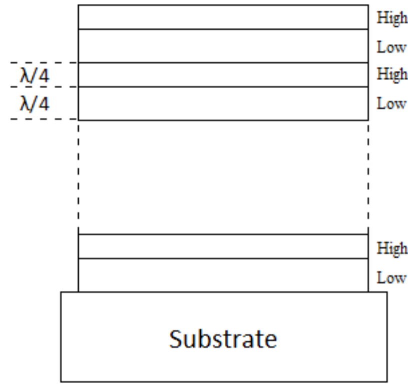

Figure 2.4: High reflectance stack

For normal incident light, the characteristic matrices M_H (for high-index, $\lambda/4$-thick layer) and M_L (for low-index, $\lambda/4$-thick layer) can be written as

$$M_H = \begin{pmatrix} 0 & \frac{i}{n_{fH}} \\ in_{fH} & 0 \end{pmatrix} \quad \& \quad M_L = \begin{pmatrix} 0 & \frac{i}{n_{fL}} \\ in_{fL} & 0 \end{pmatrix}, \tag{2.64}$$

Therefore, the characteristic matrix for one pair becomes

$$M_{HL} = M_H M_L = \begin{pmatrix} -\frac{n_{fL}}{n_{fH}} & 0 \\ 0 & -\frac{n_{fH}}{n_{fL}} \end{pmatrix} \tag{2.65}$$

For the coating composed of N number of pairs, by using the relation

$$M = \underbrace{(M_H M_L)(M_H M_L)...(M_H M_L)}_{\text{N-times}} = (M_H M_L)^N = {M_{HL}}^N \tag{2.66}$$

the characteristic matrix can be found as

$$M = \begin{pmatrix} -\frac{n_{fL}}{n_{fH}} & 0 \\ 0 & -\frac{n_{fH}}{n_{fL}} \end{pmatrix}^N = \begin{pmatrix} \left(-\frac{n_{fL}}{n_{fH}}\right)^N & 0 \\ 0 & \left(-\frac{n_{fH}}{n_{fL}}\right)^N \end{pmatrix}. \tag{2.67}$$

By using new matrix elements, the reflection coefficient can be found as

$$r = \frac{n_o(-n_{fL}/n_{fH})^N - n_s(-n_{fH}/n_{fL})^N}{n_o(-n_{fL}/n_{fH})^N + n_s(-n_{fH}/n_{fL})^N}. \tag{2.68}$$

When we multiply both the numerator and denominator by $\frac{(-n_{fL}/n_{fH})^N}{n_s}$, we can find the reflection coefficient as

$$r = \frac{\frac{n_o}{n_s}\left(-\frac{n_{fL}}{n_{fH}}\right)^{2N} - 1}{\frac{n_o}{n_s}\left(-\frac{n_{fL}}{n_{fH}}\right)^{2N} + 1} \tag{2.69}$$

and the reflectance as

$$R = \left(\frac{\frac{n_o}{n_s}\left(-\frac{n_{fL}}{n_{fH}}\right)^{2N} - 1}{\frac{n_o}{n_s}\left(-\frac{n_{fL}}{n_{fH}}\right)^{2N} + 1}\right)^2. \tag{2.70}$$

2.3.3 Edge Filters

Often, in systems using polychromatic light, the filtering is necessary to block undesired wavelength range. The edge filters divide the spectrum into two parts; one includes longer wavelengths than the selected wavelength and the other include shorter ones. They transmit one part while they reflect or absorb the other. Depending on which part is transmitted, the filter is named long wave pass or short wave pass. Usually, the edge filters use interference effect instead of absorption and they are called interference edge filters.

CHAPTER 3

THIN FILM PRODUCTION

3.1 Thin Film Processing

There are different applicable processes to coat optical components with thin layers. Basically, all of them include three main steps. The first step is obtaining the appropriate atomic, molecular or ionic form. The second is transporting these atomic, molecular or ionic forms to the surface of substrate through a medium. And the final basic step is formation of solid deposit on the substrate by condensation of the material directly or via a chemical reaction. In the formation of thin films, when the material impacts the substrate surface, it loses its velocity component which is normal to the substrate surface and the physical adsorption occurs [7]. Since there is not thermal equilibrium between the substrate and adsorbed materials initially, the materials move over the surface, interact between themselves and generate bigger clusters. Depending on the deposition factors, the clusters may decompose in time or collide with other adsorbed materials and grow in size. When they reach a certain size, they form thermodynamically stable nuclei. These new nuclei can grow in both directions; parallel or perpendicular to the substrate surface, but generally, the lateral growth rate is higher than the perpendicular growth rate [7]. As the nuclei grow, they form islands which will coalesce to compose bigger islands. Some factors changing the surface mobility like substrate temperature affect this step. Finally, the large islands grow and fill the uncovered substrate surface to form continuous film. Figure 3.1 shows the initial stages of the film growth that depend on the surface of substrate and the thermodynamic parameters of deposition. Volmer-Weber type is the island type, Frank-van der Merve type is layer by layer type and Stranski-Krastanov type is the combination of the two.

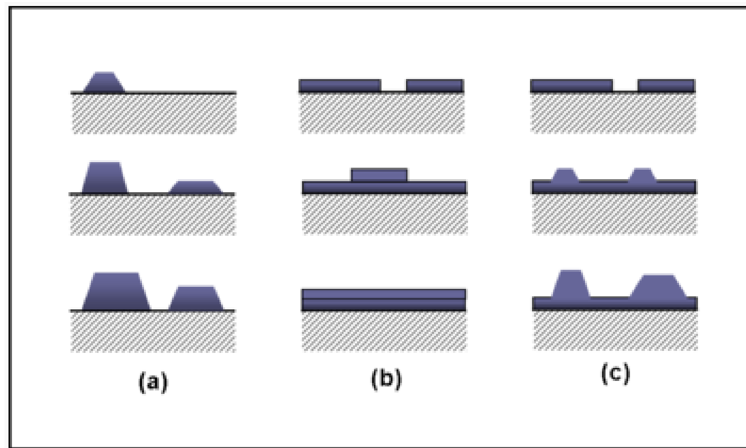

Figure 3.1: Cross-section views of the early stages of film growth

(a)Volmer-Weber growth mode by nucleation and agglomeration of islands, (b) Frank-Van der Merwe growth mode by layer-by-layer and (c) Stranski-Krastinov growth mode by combination of the two

The production of thin films involves a number of interdependent stages. The stages are:

- Selection of the substrate
- Specifying important properties of the substrate surface
- Preparing the substrate surface by cleaning and sometimes by changing the surface morphology
- Selection of the coating material or materials
- Decision of the production process to obtain long term stable and reproducible coating
- Defining the process parameters and parameter limits

After production, the characterization techniques should be developed to determine the properties and stability of the coating and also to enhance the coating with reprocessing. In the production of multilayer optical coatings, the design is another important and difficult work to obtain the component that has desired optical properties. To make a good and producible coating design, it is important to know the optical and chemical properties of substrate and coating materials. The properties of deposited thin film are determined by different parameters. The factors that affect the film properties can be summarized in four headings.

Substrate Surface: Surface morphology, mechanical properties, surface chemistry, outgassing, surface contamination are some substrate properties that can affect the morphology, structure, performance and adhesion of the film. Contaminants can be defined as any materials that get involved the film formation and in this way influence the film properties and film stability in an undesirable way. Both the amount and the type of the contaminant are important and should be reduced to an acceptable level by cleaning process. The surface cleaning can be done in two ways; external cleaning before deposition process and/or in situ cleaning in the deposition system.

Deposition Process and System Geometry: The topographical properties and structure of formed thin film depend on selection of deposition technique, gaseous contamination, angle of incidence and other deposition parameters such as temperature of substrate, source and kinetic energy of coating materials and chemical nature. These parameters are determinant of the deposition rate, the surface mobility, the level of impuritym etc. and therefore play an important role in the physical structure of the thin film.

Details of Film Growth and Intermediate Processing: The factors such as oxidation between layers, ion bombardment, nucleation of adatoms, surface mobility of adatoms, and reaction with deposition ambient also affect the film properties.

Post-deposition Processing and Reactions: Chemical reactions between film surface and ambient gases, interfacial degradation, corrosion can damage the coating. Sometimes, after deposition, corrosion occurs under atmospheric conditions due to the property of uppermost film material so the selection of the topcoat material is critical.

3.2 Thin-Film Deposition Techniques

Thin film deposition processes can be broadly divided into two categories as chemical vapor deposition (CVD) and physical vapor deposition (PVD).

3.2.1 Chemical Vapor Deposition

Chemical vapor deposition (CVD) is a method in which the material to be deposited is vaporized and reacted with other vapors, gases or liquids including the required constituents at

the heated substrate surface. The reactants can be activated by different energy forms such as heat (thermal CVD), photon (photo-assisted CVD), or plasma (plasma-enhanced CVD). Also, CVD processes can be classified by process parameters like operating pressure or precursor type. Most commonly used CVD types are atmospheric pressure CVD, low-pressure CVD, metal-organic CVD, metal-organic vapor phase epitaxy (MOVPE), and chemical beam epitaxy (CBE).

Different kinds of materials; metals, nonmetallic elements like silicon and carbon, or compounds containing oxides, nitrides, carbides and many others, can be manufactured by CVD and so it is an important process in the production of coatings, powders, fibers, semiconductors, some wear-resistant parts and in many other optical and electrical applications. Generally, CVD process needs relatively high temperature ($\sim 1000\,^{\circ}$C)[7]. Especially, the substrate temperature is critical for the process since it determines which reactions will take place. Conventional CVD processes include the following basic steps;

- Vaporization and transport of the precursors into the reaction chamber
- Gas phase reactions that form reactive intermediate species and gaseous by-products
- Adsorption of the gaseous reactants on the heated substrate surface
- Chemical reactions at the gas-solid interface to produce the deposit and by-product species
- Diffusion of the deposits along the hated surface and growth of the film
- Transportation of unreacted precursors and by-products away from the chamber

A schematic illustration of the basic conventional chemical vapor deposition process steps are shown in Figure 3.2.

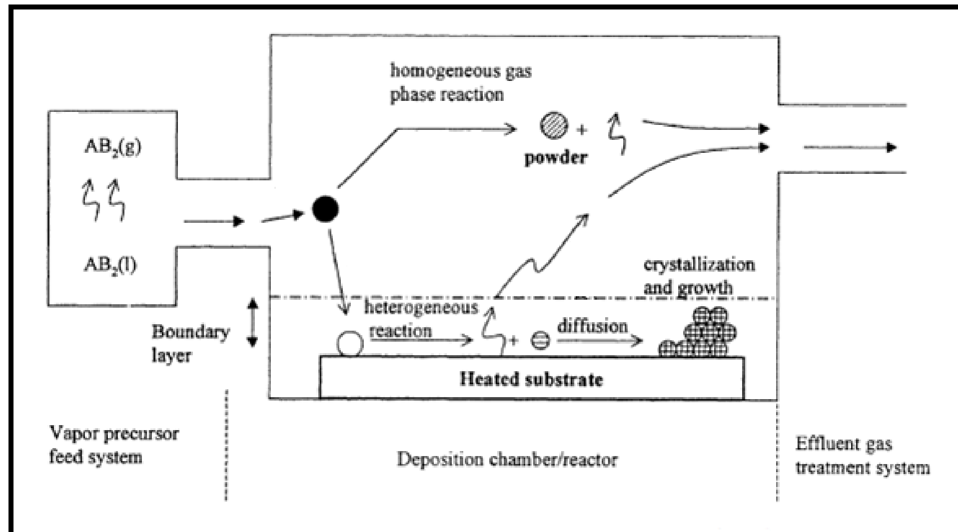

Figure 3.2: Conventional chemical vapor deposition process [8]

The mass transportation, thermodynamic and kinetic considerations, the chemistry of the reaction and the process parameters such as pressure, temperature and chemical activity are important factors that control the CVD process.

The most important advantage of CVD process is that it is not a line-of sight process so it can be used to coat three dimensional configurations which cannot be done by PVD processes. Also, normally, ultra high vacuum is not necessary for CVD processes and uniform, dense films can be produced by high deposition rates. On the other hand, at the operating temperature of CVD processes most substrates are not thermally stable. The progress in plasma-enhanced CVD and metal organic CVD partially fixes this problem but use of these methods tends to increase the cost. Also, often chemical precursors are hazardous and the byproducts of the reactions are toxic and corrosive. Neutralization of them also increases the cost of fabrication. In the production of optical thin films, the classical CVD processes are not preferred due to these disadvantages.

3.2.2 Physical Vapor Deposition

Physical vapor deposition (PVD) is another method used for thin film production. The process comprises of 3 basic steps:

- Vaporization of the coating material from a solid or liquid source
- Transportation of vaporized material through a vacuum or plasma environment
- Condensation of the material on the substrate surface.

When produced thin film will include metal oxides, carbides, nitrides or other such materials, the target will comprise of the metal. The vaporized target material then reacts with the proper gas such as oxygen, methane and nitrogen at the transportation stage and transformed into the desired material. In such cases the reaction will be another process step.

The main difference between CVD and PVD processes is that deposition occurs by chemical reaction in CVD whereas it does by condensation in PVD. The most important disadvantage of the PVD is that it is a line-of-sight process so it is not a good way to coat complex-shaped surfaces. On the other hand, PVD is a successful process in the production of coatings including metals and refractory compounds with its lower process temperatures. The lower process temperature provides no distortion on the materials. These properties make PVD processes ideal for optical coatings.

There are different techniques of PVD processes and most used ones are briefly explained below.

3.2.2.1 Sputtering

In PVD processes based on sputtering, a target (or source) is bombarded with accelerated atomic-sized particles, typically Ar gas ions, in a high vacuum environment. Surface atoms are physically ejected from the target surface by momentum transfer and they move to the substrate surface to be deposited. Schematic representation of sputtering process is shown in Figure 3.3.

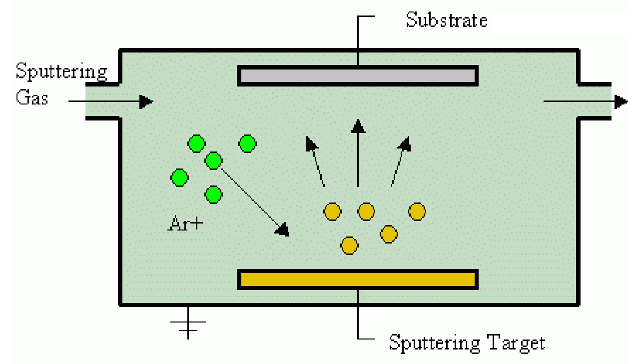

Figure 3.3: Basic scheme of sputtering process

Unlike CVD or other PVD process evaporation, the sputtering is a non-thermal process. In sputtering, the acceleration of particles can be done by a high voltage, plasma or glow discharge. The distance between the target and substrate is generally short to minimize gas phase collisions. The sputtering technique is widely used for the semiconductor and hard coating industries, reflective coatings on CDs, coatings of architectural glass and decorative and jewelry coatings.

3.2.2.2 Evaporation

In evaporation process, the target is heated in a vacuum chamber. The vaporized materials go to the substrate surface and condense to form thin film. This process requires high vacuum environment to remove all background gases and small particles which can affect the film quality. Typically, the gas pressure range is 10^{-5} - 10^{-9} Torr for this process [9]. Evaporation is generally done either by resistance heating or high energy electron beam. These two types of evaporation are shown in the Figure 3.4.

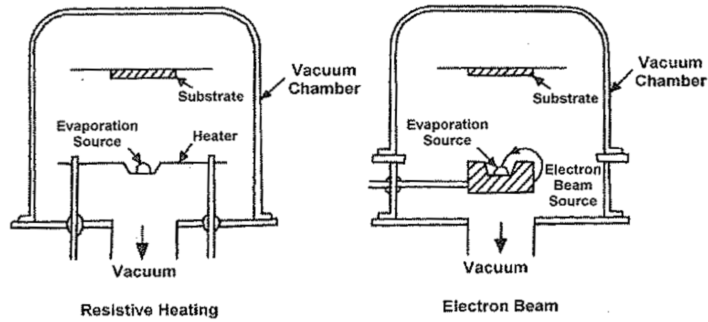

Figure 3.4: Evaporation methods [7]

Generally, in evaporation processes, there is a considerable distance between the substrate and the evaporation source in order to decrease radiant heating of substrate. Nevertheless, in the high vacuum environment, the mean free path is large in comparison to this distance and few collisions occur before condensation [10]. This causes non-uniformity in film thickness because the coating thickness over the surface varies depending on closeness to the source. To solve this problem and obtain homogenous coating, planetary (rotating) substrate holders can be used.

The evaporation technique is used for many applications such as optical interference coatings, mirror coatings, electrically conducting films, corrosion protective coatings, decorative coatings...

Other than these methods, there are different techniques used in film deposition such as arc vapor deposition or ion plating but most thin films are produced by CVD, sputtering or evaporation. The list of special features for typical processes is given in Table 3.1.

Table 3.1: The special features for typical processes [7]

Type of Deposition	Evaporation		Sputtering		CVD	
Property	Resistive heating	Electron beam	Diode	Magnetron	Pyrolysis	Plasma
Thin Film Material	Material of low melting point	Material of high melting point, refractory metals	Wide varieties of materials, compounds, refractory metals, alloys		Decomposition and/or chemical reaction of organometallic compounds or halides	
Substrate Temperature	Low		High (>300˚C)	Low (≈100˚C)	High (≈1000˚C)	High (>300˚C)
Deposition Rate	High Metal: ≈0.5-5μm/min		Low Metal: ≈0.02-0.2 μm/min	High Metal: ≈0.5-5μm/min	High Metal: ≈0.5-5μm/min	
Gas Pressure	Low (<10^{-5} torr)		High (≈0.01-0.1 torr)	Low (≈10^{-4}-10^{-3} torr)	High (1 atm)	High (≈1-10 torr)
Energy of Evaporated Atoms	≈ 0.2 eV	≈ 10-200 eV	≈ 10-20 eV	-	-	-

Almost all techniques use vacuum condition in film growth. As mentioned before, the deposition parameters including substrate temperature, deposition rate, deposition atmosphere, and substrate materials affect the nature of coating. In deposition atmosphere, sometimes, plasma and/or ion beams are used to improve the film properties. These processes are called Plasma-Assisted, Ion-Assisted or Plasma Ion-Assisted Deposition. The problems in the conventional deposition techniques such as poor adhesion, difficulties in depositing compounds or alloys and low density with voids can be overcome by plasma based methods [12]. Also, development in plasma ion assisted process enable the use of advanced plasma source (APS) that has special features like high plasma density compatibility with oxygen, and low thermal radiation to the substrate area [11]. The detailed information about these subjects is given in the next section.

CHAPTER 4

THE COATING SYSTEM

4.1 System Overview

In the production of the optical filters, plasma-ion assisted deposition method will be used. The coating system basically comprise of a vacuum unit, a cooling system (polycold cryo generator with Meissner trap), water flow units (cold and warm water circulation) and a vacuum chamber (230x137x230 cm).

As mentioned before, to obtain high quality coatings, the vacuum environment is important. It is not easy to obtain high vacuum in such a big chamber so a vacuum system having more than one pump is necessary. The vacuum system in the coating system includes vacuum pumps (rotary vane pump, roots pump, and oil diffusion pump), vacuum measuring equipments, vacuum valves and other vacuum elements like flanges or tubes. The rotary vane pump and roots pump are used to create pre-vacuum for the high vacuum pump. In this system, the oil diffusion pump is used as high diffusion pump and it provides that the pressure of the chamber becomes high vacuum level from pre-vacuum level. Inside the oil diffusion pump, the oil is heated to the boiling point with low vapor pressure and the circular metal deflectors form aligned oil vapor jets. These jets pull the gas molecules and the collected gas molecules are pumped out.

The cooling unit (Meissner trap) also helps to decrease the chamber pressure. It comprises of a cold surface (panel) inside the chamber and an external refrigerator (Polycold). The interior cryo coil is directly connected to the Polycold. The system is a closed loop and the working principle depends on the condensation of water on a cold surface. The cold trap shortens the pumping time by adsorbing the water vapor in the chamber.

The system can have pressure $\leq 8x10^{-6}$ mbar with active Meissner trap for ~45 minutes pumping time. For longer pumping time, it can reach $\leq 8x10^{-7}$ mbar. The cleanliness of the chamber affects the pumping time or the final pressure.

The coating system has two water flow units; one is cold water unit (chiller) and the other one is warm water unit. During the process, the cold water operation takes place to remove heat building up in the components. Thus, it is provided that the components are not affected by heat and they continue to work properly. The warm water operation is activated at the end of the process, before venting. The components are heated by warm water and kept warm when the chamber is under atmospheric conditions. In this way, water condensation on the components surface is reduced and so pump down time is shortened for the next process.

The vacuum chamber is a place where the process takes place and includes important units so it is better to examine this subject in a new title.

4.2 The Vacuum Chamber

Basic design of the vacuum chamber is shown in Figure 4.1.

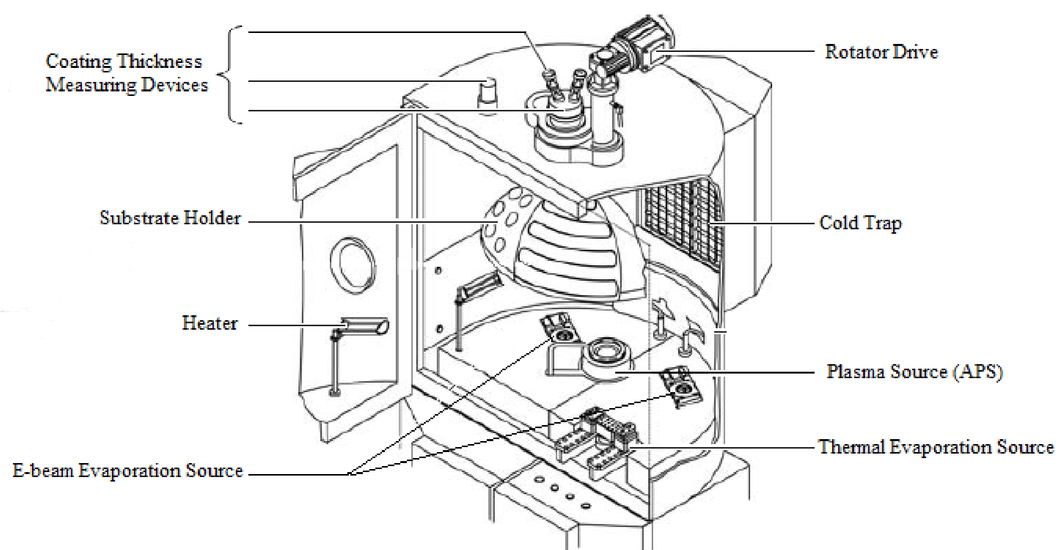

Figure 4.1: Vacuum chamber

It has basically two e-beam source, one thermal evaporation source, plasma source (APS), heaters, substrate holders, thickness measurement systems and shutters.

The substrates are mounted in substrate holders which are connected to a rotator drive. As mentioned in Chapter 3, rotational holders provide uniform coating of all substrates. Also, to make coating homogeneous, distribution shutters (masks) can be used in front of the substrate holders. The main purpose of the distribution shutter usage is to block the areas of high material concentration. In this way, the evenness of the coating can be improved. The place, shape and size of the distribution shutters can vary depending on the design of the chamber. In our vacuum chamber, the distribution shutters mounted on substrate holders are close to the substrate surface and they are in the shape of leaf.

The materials can be evaporated both by resistive heating or e-beam. In the system, thermal evaporation unit has an electrically conductive container in the form of boat. When it is heated resistively, the material inside the container is evaporated. In the production of the filters, e-beam evaporation method which will be explained in detail in the next subsection has been used. In the chamber, there are two e-beam source and two crucibles. The first crucible has one pocket which can only include one type of material and the other has 6 pockets in which different types of coating materials can be put. Both crucibles can rotate and they are water-cooled since at high temperatures many oxides react with refractory metal basins. In the chamber, there are 4 protection shutters that cover evaporation sources (crucibles and thermal evaporation container) and also plasma source. They are used to block or unblock the evaporated material or plasma. The shutter above the evaporation source can be closed until the uniform deposition rate is obtained. When the deposition time is up, the shutter enables the rapid blocking of redundant material.

Often, substrate heating is necessary before the start of the process. The substrates can be in contact with a heated fixture or radiant heating from a hot source can be used to heat up the substrates. In this coating system, three heating circuits are mounted on the chamber walls and on the chamber door to heat substrates from below. Each heating circuit has a pair of ceramic heaters of 2.6 kW each. In the vacuum chamber, the most important units are electron beam source, advanced plasma source and thickness measurement unit. Therefore, it is better to examine these subjects in detail.

4.2.1 Electron Beam (e-beam) Evaporation Source

Focused high energy electron beams can be used for the evaporation of a wide variety of materials including low vapor pressure metals, refractory metals and alloys. By e-beam evaporation, high deposition rate can be reached because a large amount of heat is concentrated on a very small area [13]. An e-beam evaporation unit mainly consists of an electron beam source, a permanent magnet, an electromagnet and a crucible with a pocket or pockets. The structure of the e-beam evaporation source that is used in this coating system is shown in Figure 4.2.

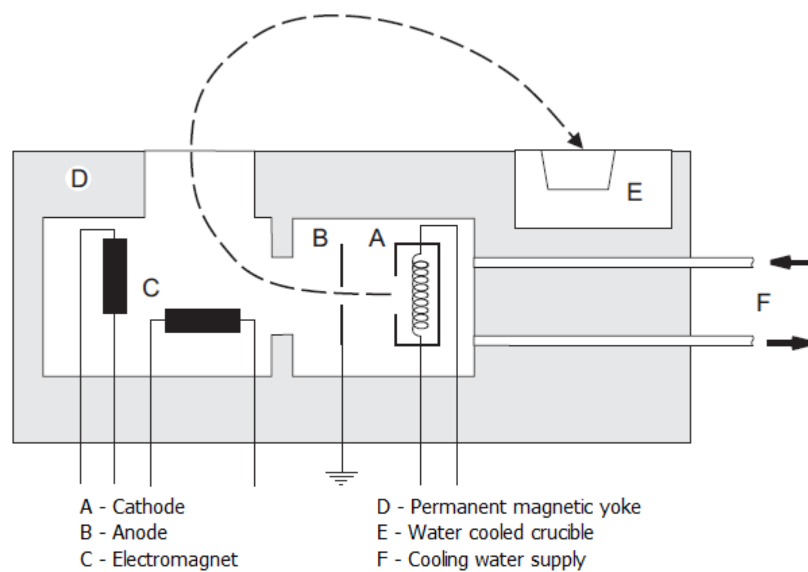

Figure 4.2: The schematic representation of the e-beam evaporation source

To create free electrons, the filament inside the e- beam gun is heated by AC current. The filament begins to emit free electrons when it becomes hot enough and so, in the vicinity of the filament, an electron cloud occurs. To accelerate these electrons, an electric field is created by applying negative voltage to the filament (cathode) and positive voltage to a metal plate with a hole in the middle (anode shown as B in the Figure 4.2). The electric field created accelerates electrons from cathode to the anode. The anode stops some of these electrons but a number of them can pass through the hole in the middle of the anode and so a beam of free electrons is generated. Then, the e-beam is guided towards the coating material in the pocket

of crucible by the static magnetic field that is created by permanent magnetic yoke shown as D in Figure 4.2. Electromagnet shown as C in Figure 4.2 consists of two coils positioned at right angles to one another. This electromagnet creates a variable magnetic field and so enables the movement of the impact point of e-beam on the target surface. The magnetic field can be altered by regulation of the coil currents.

When e-beam hits the target surface, the kinetic energy of the beam is transformed into heat (thermal energy) that vaporizes the material. Then, the evaporated material is deposited as a thin film on the substrate surface. The evaporation rate affects the quality of the coating and can be regulated by altering the e-beam intensity. The intensity of the generated heat is too high so to prevent melting of the crucible, it must be water cooled.

4.2.2 Advanced Plasma Source (APS)

In the e-beam evaporation technique, the problem of poor packing density of the coated films arises due to the low energy of the condensing particles. To improve the film properties, the processes with higher particle energies are needed. In ion assisted deposition process, momentum transfer from the incoming ions to the evaporated materials takes place and the mobility of these particles is increased. Therefore, higher packing densities and better mechanical properties can be obtained. Plasma ion assisted deposition is a useful way of producing coatings with high packing density and excellent uniformity over large substrate surfaces [14].

In the production of the filters, plasma ion-assisted deposition with an advanced plasma source (APS) that has some special features like compatibility with oxygen, high plasma density and low thermal radiation is used. The principle of operation and the structure of the APS are shown in the Figure 4.3 .

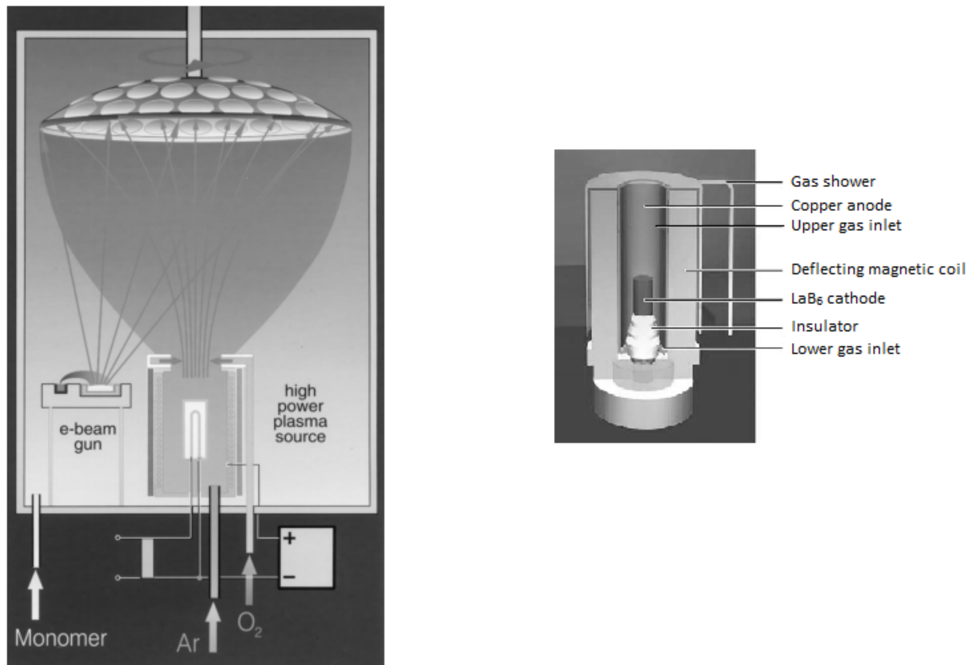

Figure 4.3: Operation principle of the plasma ion-assisted deposition and cross section of the APS [14], [15]

The plasma source is placed in the center of the chamber bottom as shown in the figure and it is based on a cylinder shaped, large-area lanthanum hexaboride (LaB_6) cathode that is surrounded by a cylindrical, water-cooled, copper anode tube. The cathode is heated by a graphite heater to a temperature of ~1500 °C. A DC voltage is applied between anode and cathode and by this way glow discharge plasma that supplied with a noble gas like argon (Ar) is created. The deflecting magnetic coil that surrounds the anode tube affects the mobility of the plasma electrons. As it increases the mobility in the axial direction, it strongly decreases the mobility in the radial direction. Therefore, electrons spiral along the magnetic field lines and the plasma is extracted towards the substrates [14].

The APS is electrically insulated from the chamber ground. The plasma acquires a positive self-bias voltage with respect to the substrate holder and to the chamber walls due to the high mobility of the electrons. The ion energy is determined by the self-bias voltage between chamber ground and anode and the magnitude of the bias voltage depends on the magnetic field strength, the applied discharge voltage and the pressure of vacuum chamber. The momentum transfer between the accelerated plasma ions and condensing film molecules

increases the surface mobility and so the packing density of deposited film. Zöller et al [23] have proved the positive effects of the plasma on coatings. According to their studies, the reflectance curves of single layer SiO_2 and TiO_2 coatings that measured under vacuum and on atmosphere after venting are different. The moisture penetration into the film causes a shift in the curve. The reason of the moisture penetration is the low packing density. When the same coatings are deposited with APS, no shift is observed.

Improving packing density is not the only effect of the plasma. It can be used for in-situ cleaning at the start of the process. If the ions created in the plasma source bombard the substrate surface before the deposition, the impurities and particles sitting on the surface get etched away. This improves the bonding between the depositing atoms and the substrate surface. The removed particles are pumped away with the working gas or stick on the chamber walls. Ion bombardment increases the substrate temperature [12] and this improves the adhesion further. During the process, plasma also provides an even temperature distribution on the substrates.

In addition, plasma is used to dissociate the reaction gas in the reactive coating processes. In the coatings with oxides, additional oxygen can be needed but it can only support the process when it is present in the disassociated form. When a flow of oxygen is directly sent over the plasma source, the ions created in the plasma break off the molecules and accelerate the oxygen ions towards the substrate surface.

In the system, there are two gas inlets in the APS unit. The argon gas coming from the lower gas inlet shown in Figure 4.3 affects the resistance and so the voltage difference between anode and cathode. To have sufficient plasma density, second gas inlet is used.

4.2.3 Thickness Measurement Systems

In order to achieve desired transmission/reflection values with resultant coating, accurate control of deposited layers thickness is essential. To measure the thickness and to stop coating when the desired thickness is reached, some form of in-situ control mechanism is required. In the coating system, on the top of the chamber, there is a measuring head that combines two measurement systems; the quartz crystal measurement and the optical coating thickness measurement. Figure 4.4 shows combined measuring head.

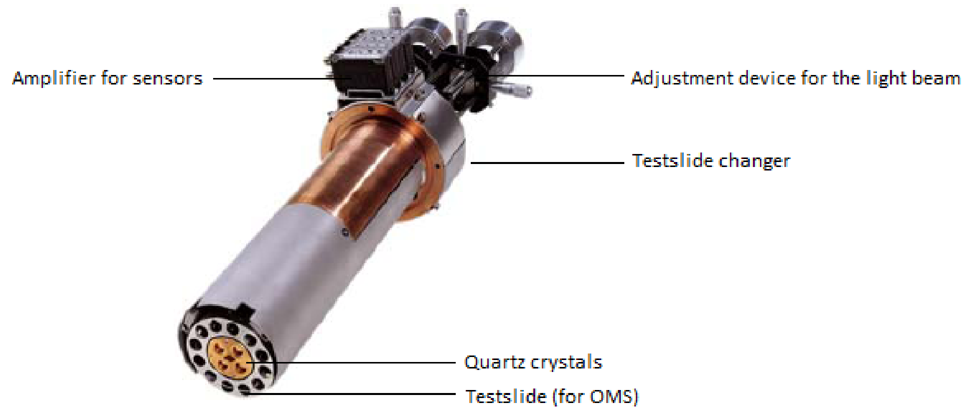

Figure 4.4: Combined measuring head

4.2.3.1 Quartz Crystal Measurement System (XMS)

Film thickness measurement with quartz crystals depends on the oscillation frequency of a simultaneously coated crystal. The principle is that as the mass of the material deposited on the surface of a quartz crystal increases, the frequency of vibration of the quartz decreases continuously. The thickness is calculated by using the change in the oscillation frequency and physical properties of the coating material (like density).

The quartz crystals oscillate at high frequency ($\sim$ 6 MHz) with the help of an oscillator. The oscillator and the measuring head (shown in Figure 4.4) including 4 quartz crystals are located in the vacuum chamber. The other part of the module, a microprocessor control, which is connected in series with the system control, is placed on the switch cabinet.

4.2.3.2 Optical Monitoring System (OMS)

The optical layer thickness measuring unit determines the thickness by means of the reflection or transmission measurement of the coating. The measurement is carried out on a test slide placed in the measuring head. The test slide holder divides the test slide into 12 measuring position as shown in the Figure 4.4. The test slide changer changes the measurement position during the process. The light beam coming via optical fiber can be set by an adjustment device

so that the light focuses at the center of the measurement position. The light reflected from the test slide surface goes into the receiving optical fiber.

The functioning principle is based on the fact that as the coating thickness increases, the intensity of reflected light (monochromatic light) changes. Figure 4.5 shows the reflections that takes place on a coated test slide. The refractive indices of test slide and coating material are n_g and n_f respectively and the thickness of the coating is d.

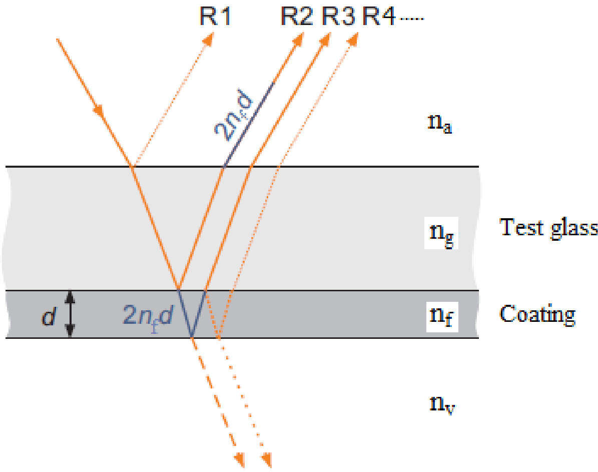

Figure 4.5: Reflections from coated test slide

The individual reflected light intensities are added up to obtain the total intensity; $R_{tot} = R_1 + R_2 + R_3 + R_4 + ...$ The path difference given by Eqn (2.2) reduces to $2n_f d$ for near normal incident light. For the light going from a medium to a denser medium, an additional $\lambda/2$ phase shift occurs. The maximum intensity of total reflection is achieved when the phase difference is equal to m times $\lambda/2$ where m is any positive integer.

$$n_f d = m\frac{\lambda}{4} \tag{4.1}$$

The thickness measurement with OMS depends on the turning point condition which is met at regular intervals. The reflected light beam intensity passes through different maximum and minimum points as the coating thickness increases during the process and so the curve obtained by OMS has a periodic structure over time. To use this method, a certain control

wavelength λ should be selected.

According to Equation (4.1), the thickness of the coating depends on the refractive index of the coating material n_f and the wavelength λ. Therefore, it can be easily controlled by using the curve obtained from the reflection measurement when both quantities are known. The change in the obtained curve with the increasing coating thickness is shown in the Figure 4.6.

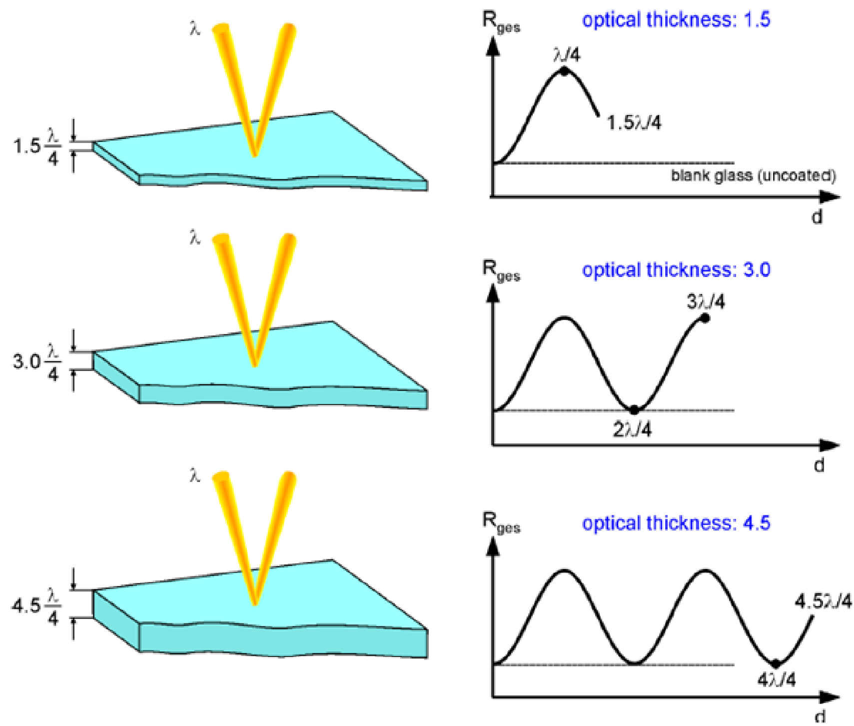

Figure 4.6: Thickness-dependent curves obtained by OMS

To terminate the deposition process with the exact desired coating thickness, the cut-off point should be positioned in a favorable area where the curve shows a steep gradient as shown in the Figure 4.7. The cut-off point should come after the first turning point in order the OMS to be able to make corrections. Also it should not be in the edges of the turning point to decrease the errors caused by signal noise. The control wavelength can be chosen so that the cut-off point goes into the favorable area.

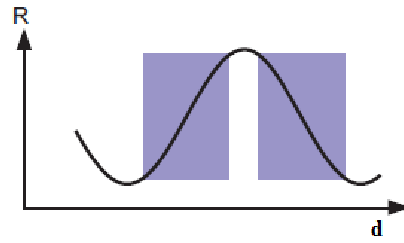

Figure 4.7: Favorable areas for cut-off point

The basic structure of the OMS unit is shown in the Figure 4.8.

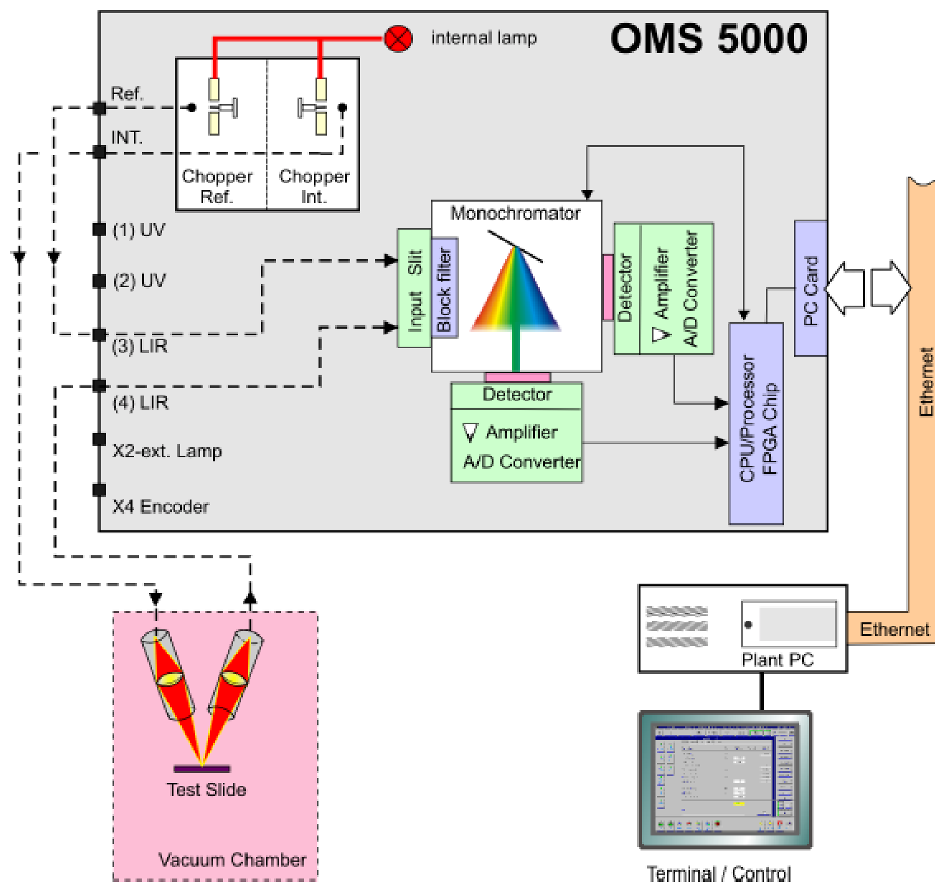

Figure 4.8: Basic structure of OMS

A halogen lamp creates a light beam with continuous wavelength. The light is divided into two fiber optical cables; reference cable in which the light is directly sent to a step motor-

controlled monochromator and measurement cable in which the light is sent to the test slide. The light reflected from the test slide surface is sent to the monochromator via another fiber and the control wavelength is filtered out from the continuous spectrum at the monochromator. The altered light beam is sent to a detector that converts the incoming light signals to an electrical voltage. There are two detectors in series with the monochromator; a silicon detector for visible range and a photomultiplier for UV range. The generated electrical signal is processed and sent to the system control of the coating system.

The measured value consists of the measurement quantities as follows

$$M.V. = \frac{Int.Signal - DarkInt}{Ref.Signal - DarkRef} xC \tag{4.2}$$

where C is the calibration factor with that the refractive index of the test slide and the gain factor are taken into account.

4.2.3.3 Tooling Factor

The term tooling factor is used to describe the ratio between the actual thickness of the deposited layer on the substrates and the thickness monitored by the thickness measurement systems. The difference in thicknesses is caused by mainly two reasons:

- The substrates and the measuring head (quartz crystal and test slide) are located at different positions in the vacuum chamber.

- The substrates are covered by the distribution shutter while the quartz or test slide is not.

Therefore, the exposure to the coating materials is different for substrates and for measuring head. In addition, the angular distribution of material leaving a source is different from material to material [16]. For these reasons, the tooling factor should be calculated for each material before the process in order to compensate the possible difference in thicknesses.

A typical procedure to calculate the tooling factor of a material is to deposit a single layer with several quarter wave optical thicknesses. Then, substrates or witness pieces placed in the chamber during the process are measured by means of a spectrophotometer. The spectral shift in wavelength obtained from the comparison of design (monitor) with the resultant spec-

trophotometer measurement gives the tooling factor for that material. This factor is used to make necessary adjustments for the next run.

On the other hand, the indices of coating materials are different from the monitoring wavelength to the band of interest due to dispersion [16]. The dispersion data can also be found by the same procedure in which tooling factors are calculated and the problems caused by the inaccurate knowledge of the actual refractive indices can be solved.

CHAPTER 5

DESIGN AND PRODUCTION OF THE FILTERS

5.1 The Material Selection

The CCDs with produced filters will be used in the electronic unit of a low orbit space-camera so the coatings should be space-qualified. Temperature, radiation, atomic oxygen and micro-meteoroid effects [17] are main factors that can degrade the optical properties of coating in the space environment, therefore; the material selection becomes an important issue. For space applications, the mostly used coating materials are magnesium fluoride (MgF_2), yttrium oxide (Y_2O_3), tantalum pentaoxide (Ta_2O_5), silicon dioxide (SiO_2), titanium dioxide (TiO_2), aluminum oxide (Al_2O_3) and zinc sulphide (ZnS).

Chemical purity, physical properties and process suitability of the materials are also important in selection of coating materials in order to provide demands of the process and so to obtain the required film properties. In the production of the optical filters, two dielectric materials were used; silicon dioxide as low index material and titanium dioxide as high index material. TiO_2 SiO_2 multilayers provides broad reflectance bands due to the large difference in refractive indices.

5.1.1 Silicon Dioxide (SiO_2)

The granulate form of silicon dioxide (SiO_2) was used as target material. It has been obtained from Umicore and has 99.99% chemical purity. The first crucible consisting of single pocket was used for SiO_2 target material. When the material is exposed to the e-beam, it directly sublimates so the speed of crucible rotation is critical. If it is too fast, then the energy (heat)

will not be sufficient for sublimation. The general features of SiO_2 are shown below [18].

Table 5.1: The general features of SiO_2

Coating material	Film composition	Deposition method	Range of transparency	Refractive index at 550 nm
SiO_2	SiO_2	E-Beam	0.2 - 9 μm	1.45 – 1.46

5.1.2 Titanium Dioxide (TiO_2)

The granulate form of titanium pentoxide (Ti_3O_5) was used as target material. It has been obtained from Umicore and has 99.5% chemical purity. Titanium dioxide (TiO_2) thin film was obtained by means of reactive e-beam evaporation method which is the best way of obtaining TiO_2 layers for multilayer coatings. For the process, Ti_3O_5 was placed in a pocket of second crucible. During evaporation of Ti_3O_5, extra oxygen gas was sent to the chamber. In this way, TiO_2 layers were obtained by reactive e-beam deposition technique. If the coating includes many TiO_2 layers, then more than one pocket can be used for Ti_3O_5 target material. The typical deposition rate is 0.2-0.5 nm/s. When using coating materials like Ti_3O_5, pre-melt process is necessary before the coating process because too inhomogeneous surface of target material in the crucible causes unevenly distributions of the evaporated materials (irregular vapor clouds) on the substrate. Also, pre-melt process provides to eliminate the gas holes in the target material that cause uncontrolled out gassing and disruptions in the coating process. The general features of the material are shown below [18].

Table 5.2: The general features of TiO_2

Coating material	Film composition	Deposition method	Range of transparency	Refractive index at 550 nm
Ti_3O_5	TiO_2	Reactive E-Beam	0.4 – 3 μm	2.1 – 2.4

5.2 Tooling Factors and Wavelength-Dependent Refractive Indices

Before coating process, it is necessary to determine some parameters like tooling factor and wavelength-dependent refractive index for each material as mentioned in previous chapter.

In calculations, the spectrometric measurements of single layer coatings having a number of quarter wavelength thicknesses are used. For such a single layer, we have

$$n_f d = m\frac{\lambda}{4}$$

where n_f is the refractive index of the film, *d* is the geometrical thickness (optical thickness = refractive index *x* geometrical thickness), λ is the wavelength and *m* is the number of $\lambda/4$. To calculate refractive index n_f, both reflectance and transmittance curves of single layer can be used. If the reflectance is used, the necessary formula derived from Equation (2.57) is

$$n_f = \sqrt{n_s \frac{1+\sqrt{R}}{1-\sqrt{R}}} \tag{5.1}$$

If the transmittance is used in calculations, the necessary formulas are given as

$$r_1 = \left(\frac{1-n_s}{1+n_s}\right)^2 \tag{5.2}$$

$$r_2 = \frac{1-r_1-T}{1-r_1(1+T)} \tag{5.3}$$

$$n_f = \sqrt{n_s \frac{1+\sqrt{r_2}}{1-\sqrt{r_2}}} \tag{5.4}$$

B270 flat glasses are used as substrates and dispersion data belonging to the glass is given in the Appendix 1.

The coating system has two measurement system as mentioned before so two tooling factors should be calculated; one is geometrical for quartz crystal measurement system ($Tooling_{XMS}$) and the other is optical for optical monitoring system ($Tooling_{OMS}$). They can be calculated from the equations given below.

$$Tooling_{XMS} = \frac{d_{actual}}{d_{input}} \; Tooling_{XMS,initial} \tag{5.5}$$

$$Tooling_{OMS} = \frac{d_{testglass}}{d_{substrate}} = \frac{m_1 \lambda_1}{m_2 \lambda_2} \quad (5.6)$$

In Equation (5.5), $Tooling_{XMS,initial}$ is any number used as tooling factor for the single layer coating process. For simplicity, it is taken as 100 which means it is assumed that there is no difference in thickness between the thin films on substrate and on measurement system. d_{actual} is the geometrical thickness calculated by Equation (5.2) and d_{input} is the thickness measured by quartz crystal.

Calculations for SiO_2: Input data for SiO_2 are given in the table below.

λ_1	650 nm
m_1	3.3
n	1.465
$Tooling_{XMS,initial}$	100
d_{input}	332.13 nm

Since refractive index of the material is less than the refractive index of substrate, reflectance measurement is more suitable for the calculation. The spectroscopic measurement of single layer SiO_2 coating is shown in the Figure 5.1.

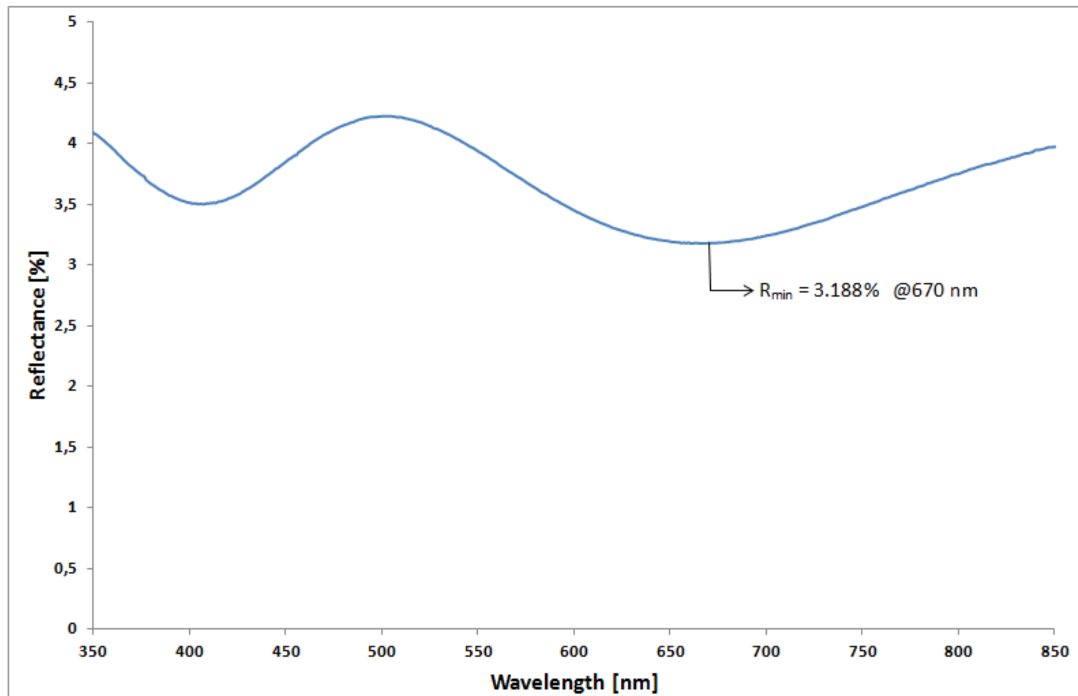

Figure 5.1: Reflection curve of single layer SiO_2 coating

As seen in Figure 5.1, R_{min} is 0.03188 at 670 nm for m=3. By using Equation (5.1) and the refractive index table of substrate given in Appendix 1 ($n_{B270}(@670nm)$=1.516927), it can be found that n_{SiO_2}=1.47525. Also, one can find that d=340,62 by using Equation (5.2). Thus, tooling factors for SiO_2 can be calculated by using Equations (5.5) and (5.6) as

$Tooling_{XMS}$	102.56
$Tooling_{OMS}$	1.067

Calculations for TiO_2: The data used for the single layer process are given in the table below.

λ_1	550 nm
m_1	3.3
n	2.35
$Tooling_{XMS,initial}$	100
d_{input}	155.37 nm

The transmission curve of TiO_2 is given in the Figure 5.2.

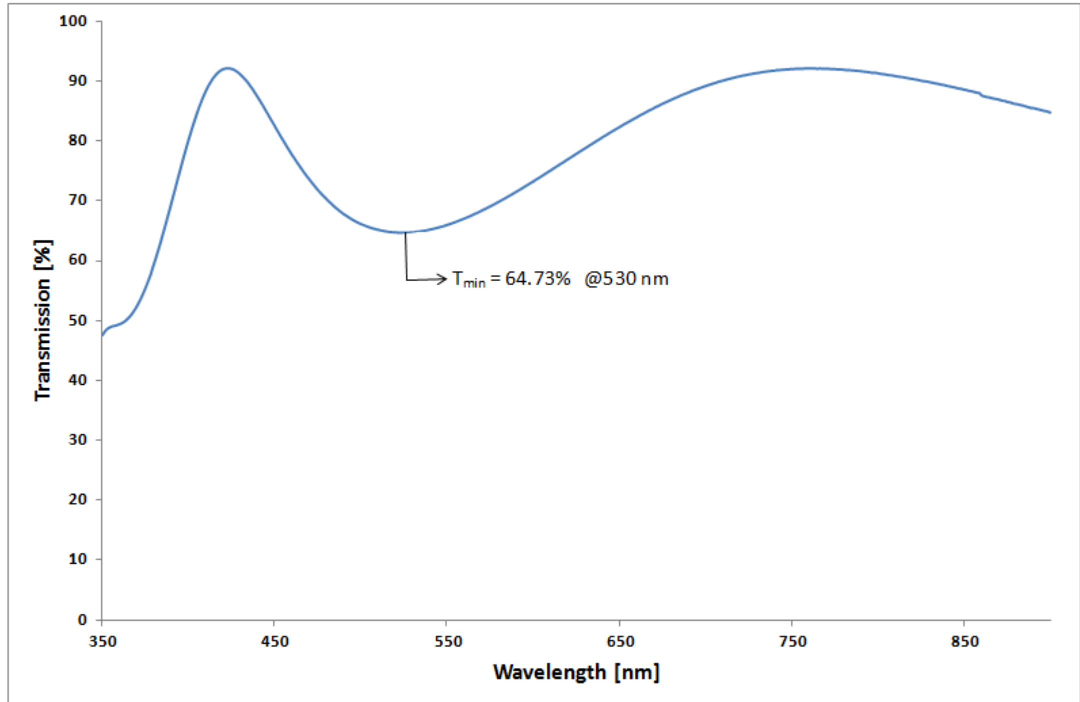

Figure 5.2: Transmission curve of single layer TiO_2

As shown in the figure, T_{min} is equal to 0,6473 at 530 nm for m=3. Since n_{B270} (@530nm)=1.523447, one can calculate r_1=0.043029 by using Equation (5.2), r_2=0.3333 by using Equation (5.3), n_{TiO_2}=2.384329 by Equation (5.4) and d=166.7135 by Equation (5.2). Therefore, tooling factors for TiO_2 can be found as

$Tooling_{XMS}$	107.3
$Tooling_{OMS}$	1.14

To obtain the same results with the design, beside the tooling factors, the dispersion data of coating materials are needed since refractive indices are wavelength dependent. It is possible to get the information belonging to the refractive indices of materials by transmission or reflection curve of single layer coating. A computer program, called MatEdit, was used to get dispersion data. It calculates refractive index n by using Cauchy dispersion relation and extinction coefficient k by using absorption coefficient . The obtained dispersion data are

shown in the graphs below.

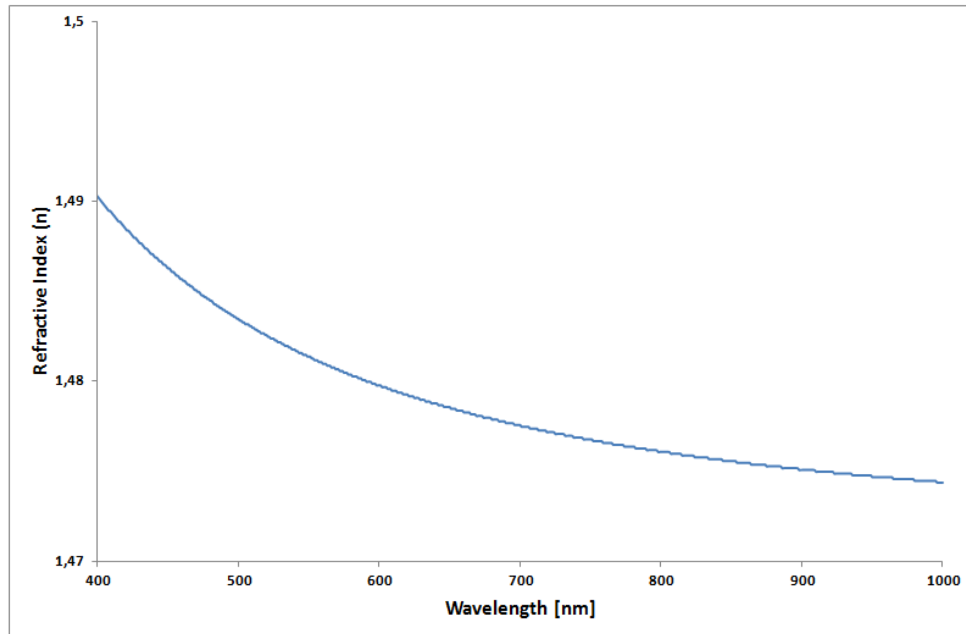

Figure 5.3: Wavelength-dependent refractive index of SiO_2

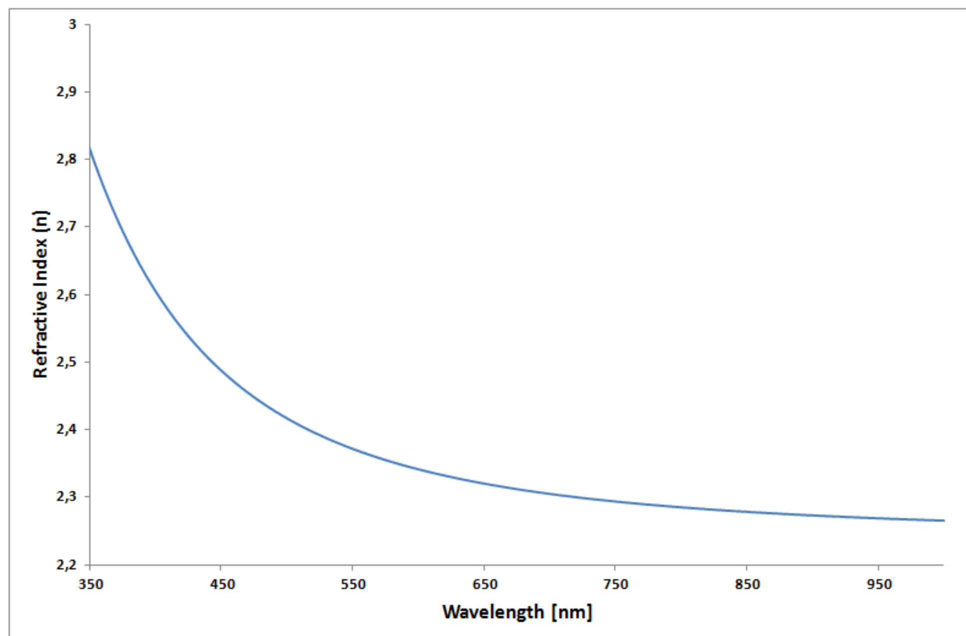

Figure 5.4: Wavelength-dependent refractive index of TiO_2

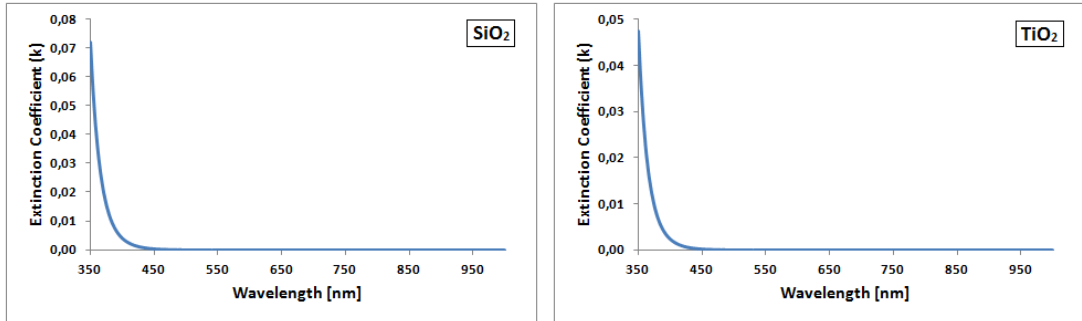

Figure 5.5: Extinction coefficients of SiO_2 and TiO_2

5.3 Design of the Optical Filters

The structure known as quarter-wave stack is the main dielectric reflecting structure. By quarter-wave stack, a limited high reflective zone can be obtained. The regions that surround this zone have relatively high transmittance but exhibit ripples. In order to convert this type of structure into an edge filter, the ripples should be reduced. The sharpness of the transition from transmitting zone to reflecting zone increases with the number of layers. However, to have a producible design, the number of layers should not be too high. Both reduction of ripples and optimization of the number of layers are not easy tasks but get easier by the help of recently developed design programs. Although the computer programs help to make the design process easier, some parameters decided by humans such as starting design, kind of optimization, thickness of the thinnest layer, number of layers, thickness of the coating etc affect the final design. In this work, OptiLayer Thin Film Software was used as design program for the filters.

5.3.1 The Design Program: OptiLayer Thin Film Software

OptiLayer is a program that offers different refinement and synthesis techniques after loading the information about target, coating materials, substrate, starting design, and other inputs. It is also possible to make a design without any starting design but the final design will be affected by this choice. The purpose of refinement and synthesis procedures is to obtain design with desired spectral characteristics by optimization of a merit function. To do this,

the number of layers, the layer thicknesses and the layer materials are changed during the procedure. The merit function (MF) is automatically constructed in accordance with user-specified targets. The merit function is represented by

$$MF = \left(\frac{1}{N} \sum \left(\frac{T_j - T'_j}{DT_j} \right)^2 \right)^{1/2} \tag{5.7}$$

where N is the total number of targets, T_j are theoretical values of the spectral characteristics, T'_j are target values and DT_j are tolerances.

The most used OptiLayer commands to optimize the design are explained below.

Refinement : The refinement procedure is used to adjust the layer thicknesses of the current design. In other words, the merit function is optimized with respect to the layer thicknesses in this process.

Needle Optimization : In the Needle optimization process, new thin layers are inserted into the design. The material of new layer is the other material than the one of the layer that the insertion takes place in the two-material situation. When more than two coating materials are loaded in design process; then, an optimal material is chosen among all materials as new layer material. In the automatic mode, the location of new layer is automatically decided and the optimal thickness for new layer is computed. The process stops when there is no possible new layer insertion to improve the current design or when it is interrupted by the user. This means that, for the current total optical thickness, an optimal solution has been obtained. To improve the merit function further, the increase in total optical thickness should be allowed.

Gradual Evolution : This synthesis tool is useful when the total thickness of the design is insufficient to have the desired value of the merit function. It can be used when the design procedure starts with simple starting design or without any starting design. Before gradual evolution process some termination criteria should be defined. During the process, a thick layer is inserted in the design if the termination criteria are not met by needle optimization. The location of this new layer can be chosen as near the incident medium, near the substrate or somewhere in the design. After thick layer insertion, the process continues with Needle

optimization and runs until one of the termination criteria has been obtained. If the termination criteria cannot be satisfied at the end of the Needle optimization process, then another thick layer is inserted and another cycle starts. The Gradual Evolution window is shown in the Figure 5.6.

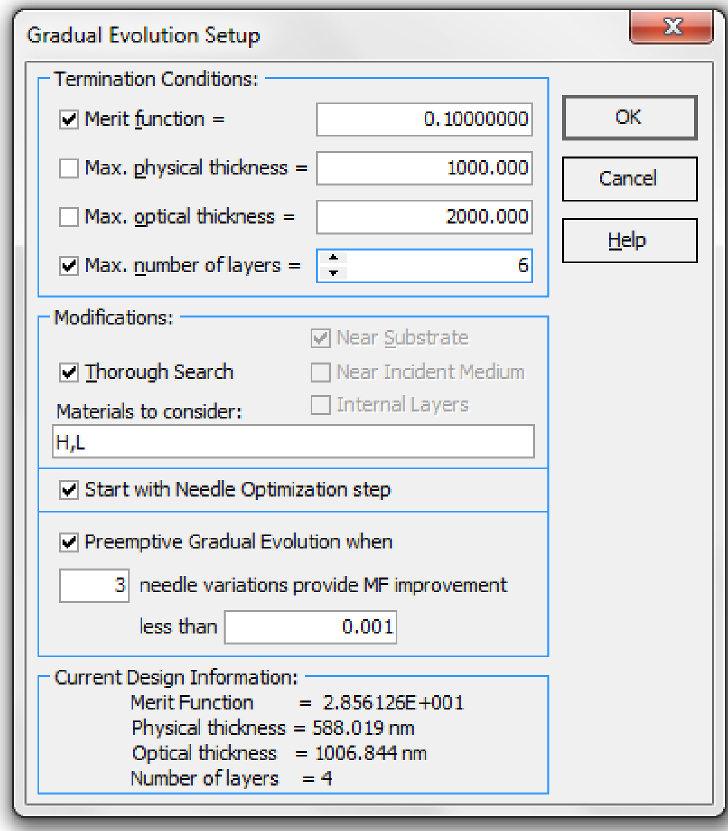

Figure 5.6: The gradual evolution window

After the desired design is achieved, there are also some synthesis processes to make the production of design easier. The final design may have too many layers or too thin layers which can cause some problems in the production process. To decrease the number of layers of the final design, design cleaner option can be used. After allowed increase of merit function (%) is defined, this option removes the layers that have small effect on the merit function value. To remove the too thin layers, more than one way can be followed. The first way is the thin layer removal option. This command removes the thin layers until one of the termination criteria is achieved. The termination criteria include merit function criterion (allowed increase

of MF) or/and thickness stop criterion (thickness of the thinnest layer). The other way to get rid of the thin layers is combining the thin layer with the previous or the next layer manually and then using refinement command.

5.3.2 The Design Procedure

To start a design, at first, some basic design parameters should be defined in OptiLayer. As light source, the uniform distribution was chosen since, in our case, the light source is the sun. Air was loaded as incident medium and glass (B270) was loaded as substrate. Then, the coating materials should be defined. Here, the dispersion data found for the materials should be loaded as shown in the Figure 5.7.

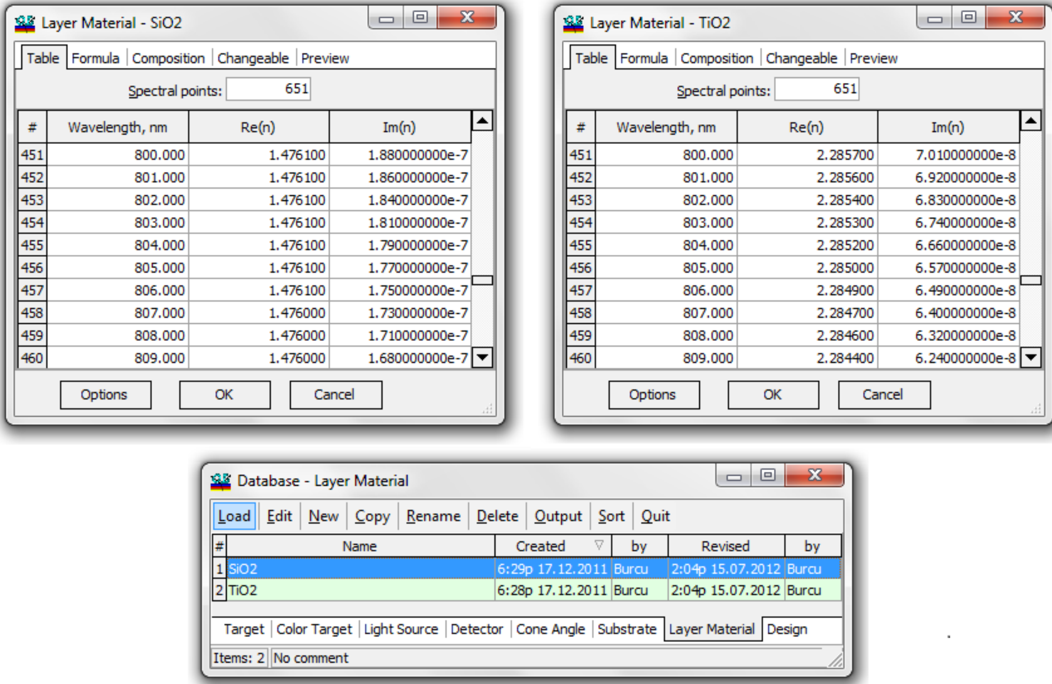

Figure 5.7: Description of coating materials

After loading these parameters, the target should be defined. In our case, the wavelength spectrum is so wide that it is not easy to obtain desired design with simple starting design. The way followed is that, at first, the design procedure was conducted for a target defined for a narrow spectrum and then, the obtained design was used as starting design for the target

defined for whole spectrum. The final design depends on the user decision because it is always possible to continue the process by adding layers. However, as the total thickness increases, the production of the design gets harder. Optimum solution should be found and when the decrease in merit function becomes insignificant the process should be stopped.

For the initial design, the form of 0.5H L H ... H L 0.5H and 0.5L H L ... L H 0.5L can be used to start designs of long-pass and short-pass filters, respectively. This representation means that all layers have equal optical (quarter wavelength) thickness except the first and the last ones which have thickness as half of the others. This notation can be simplified as $(0.5H \;\; L \;\; 0.5H)^p$ where p is number of periods of layer-stack noticed in brackets.

5.3.2.1 Design of Short-Pass Filter

At first, the target including the wavelength range between 400 - 900 nm was defined as shown in the Figure 5.8.

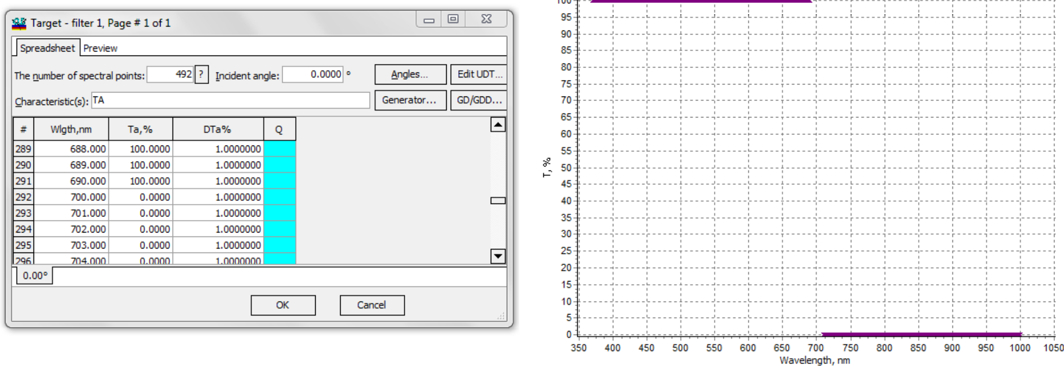

Figure 5.8: Definition of the target

Then, the starting design $(0.5L \;\; H \;\; 0.5L)^4$ was loaded as shown in the Figure 5.9.

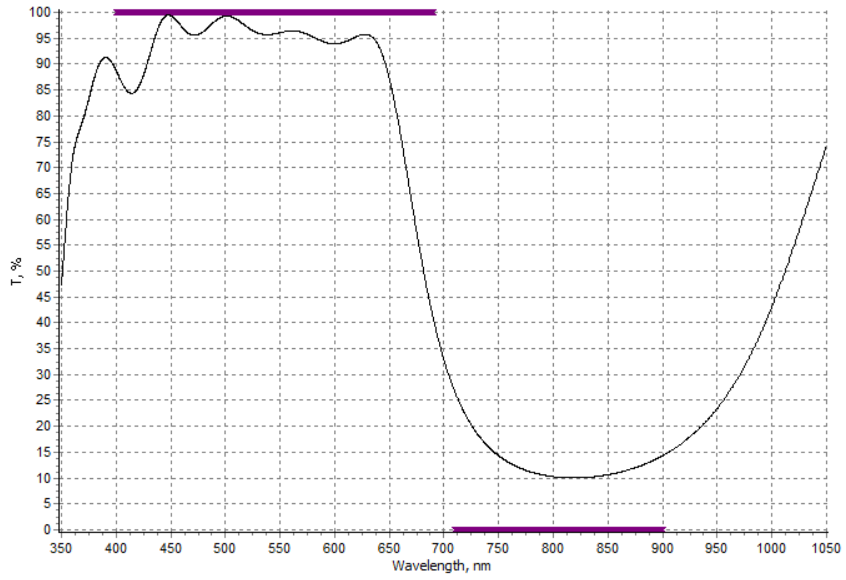

Figure 5.9: 9-layer initial design for short-pass filter

After a series of refinement, optimization, evolution procedures, thin layer removal and design cleaning procedures, the obtained design is shown in the Figure 5.10.

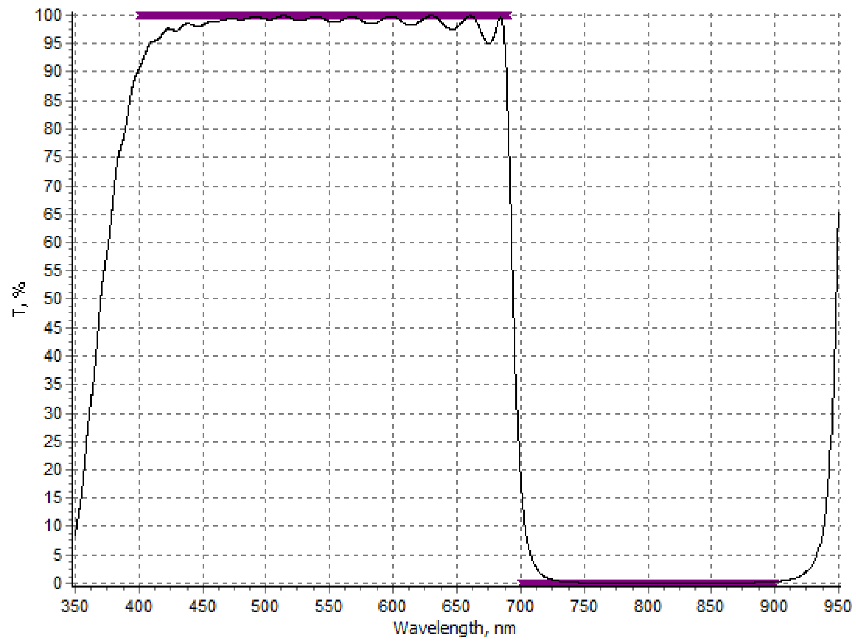

Figure 5.10: 24-layer design for narrow target

When the target is expanded to 370 - 1000 nm, the procedure can be carried on by using this design as starting design. The procedure was started with refinement and went on other commands. The final design is shown in the Figure 5.11.

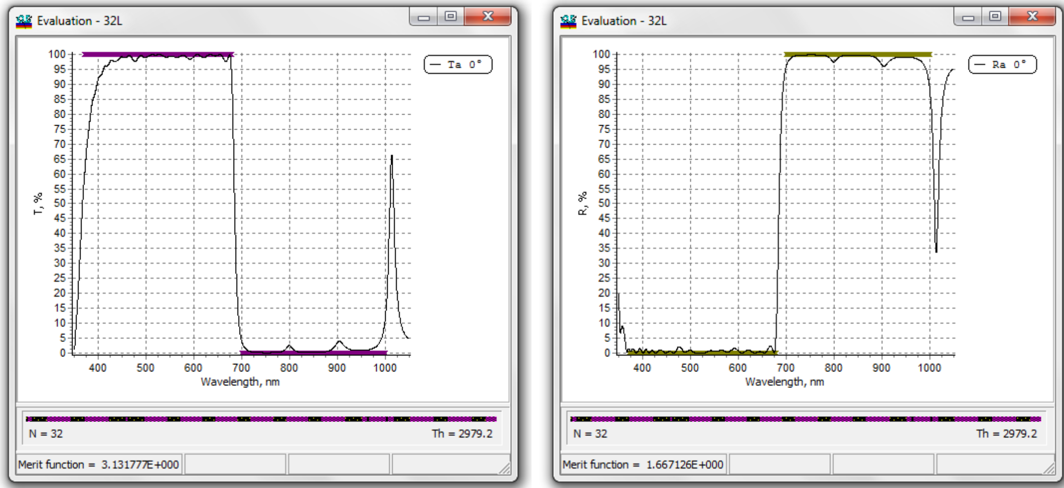

Figure 5.11: 32-layer design for short-pass filter

(the left is transmission and the right is reflection curve)

The uncoated side of the substrates causes a reduction in the transmitted zone as shown in the Figure 5.12.

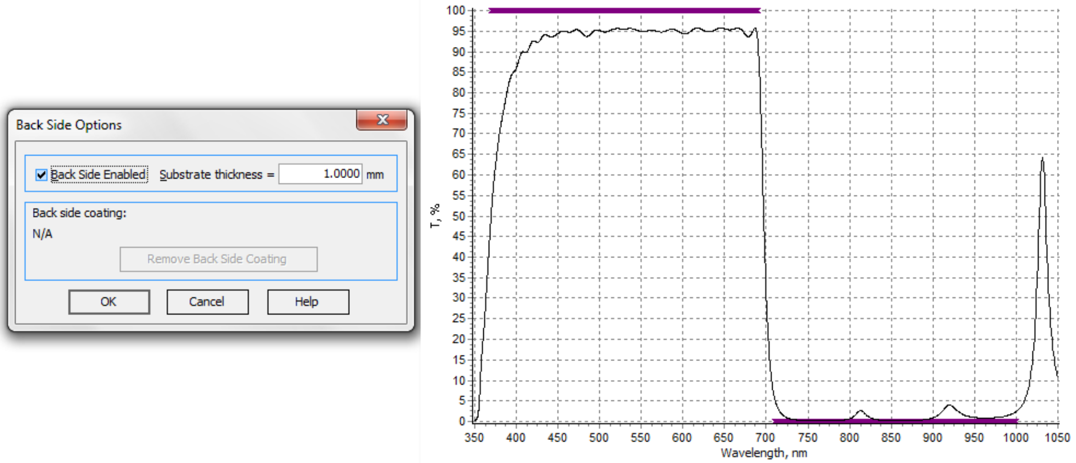

Figure 5.12: Backside effect

To minimize this backside effect, a backside coating should be designed. To design backside coating, the current design should be loaded as backside coating and new design procedure should be conducted. Since the backside coatings are not very complicated and they do not have many layers, design process can be started with gradual evolution process without any starting design. The final design for short-pass filter including both side coating designs is shown in the Figure 5.13.

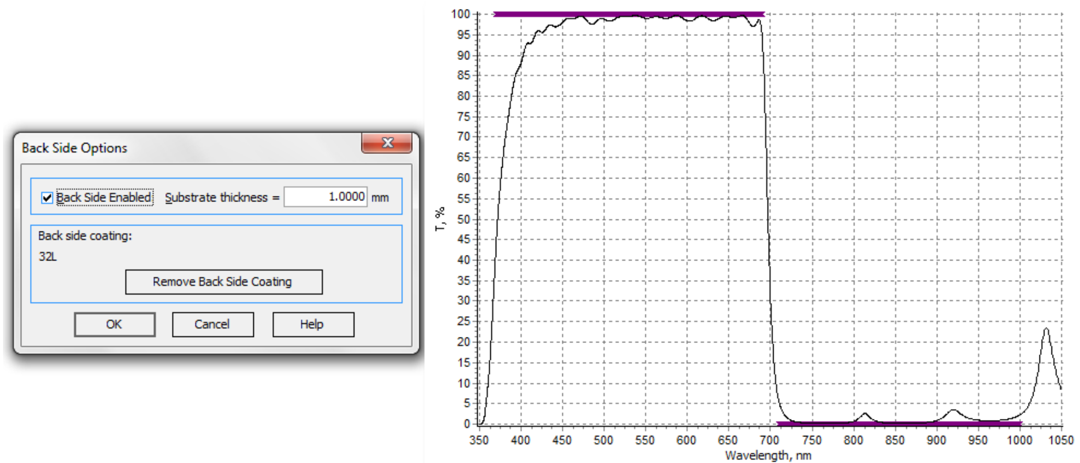

Figure 5.13: Final design for short-pass filter

5.3.2.2 Design of Long-Pass Filter

As in the short-pass filter design, the design of long-pass filter was started with loading a narrow target (450 - 900 nm). For starting design, p was chosen as 6 and the design of $(0.5H\ \ L\ \ 0.5H)^6$ shown in Figure 5.14 was used.

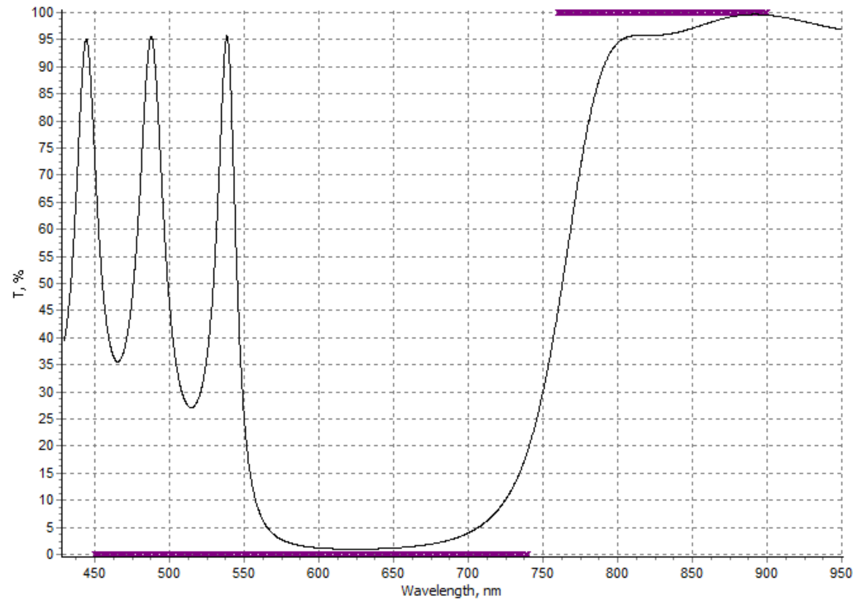

Figure 5.14: 13-layer initial design for long-pass filter

The initial design after refinement is shown in Figure 5.15.

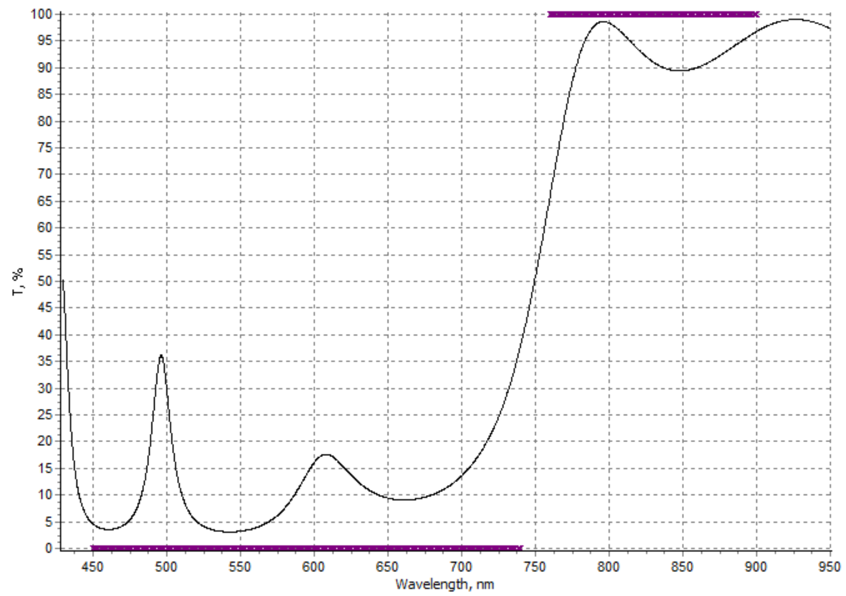

Figure 5.15: 13-layer initial design after refinement

After all optimization procedures were conducted as in the short-pass filter design process, the obtained design is shown in the Figure 5.16.

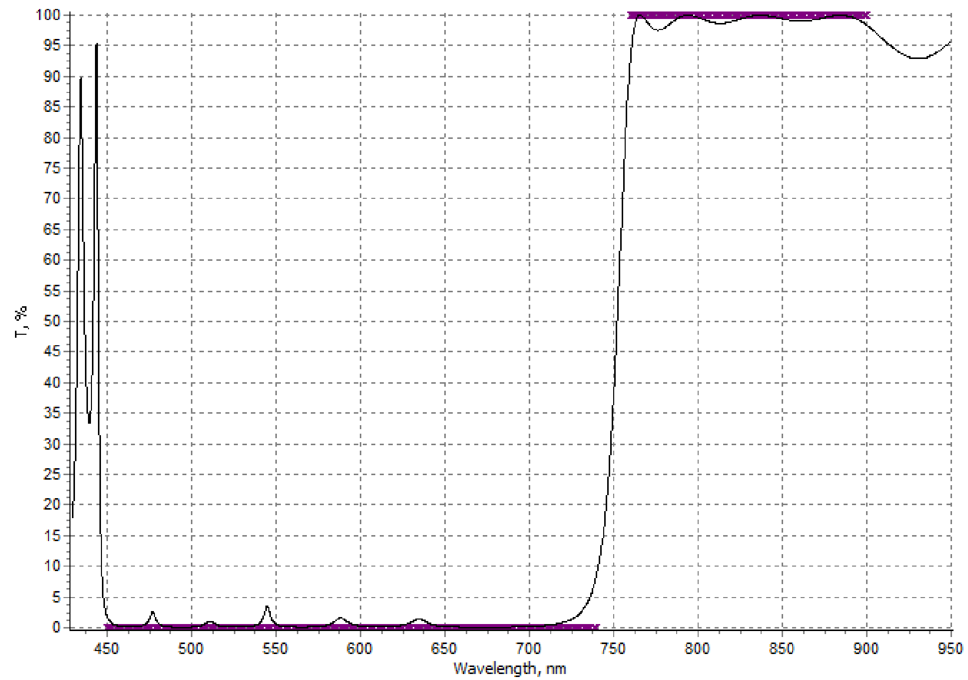

Figure 5.16: 32-layer design for narrow target

The design process continued with the extension of the target. After an array of refinement, optimization and evolution procedure, a design having too many layers was obtained (Figure 5.17).

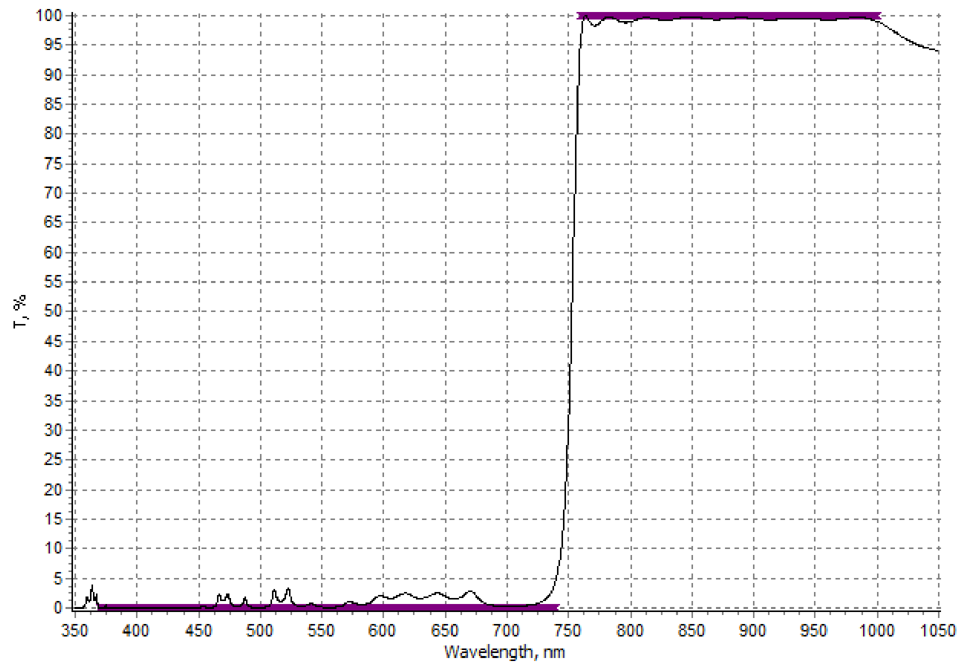

Figure 5.17: 64-layer design

The final design that was achieved after removing thin layers and cleaning the design is shown in the Figure 5.18.

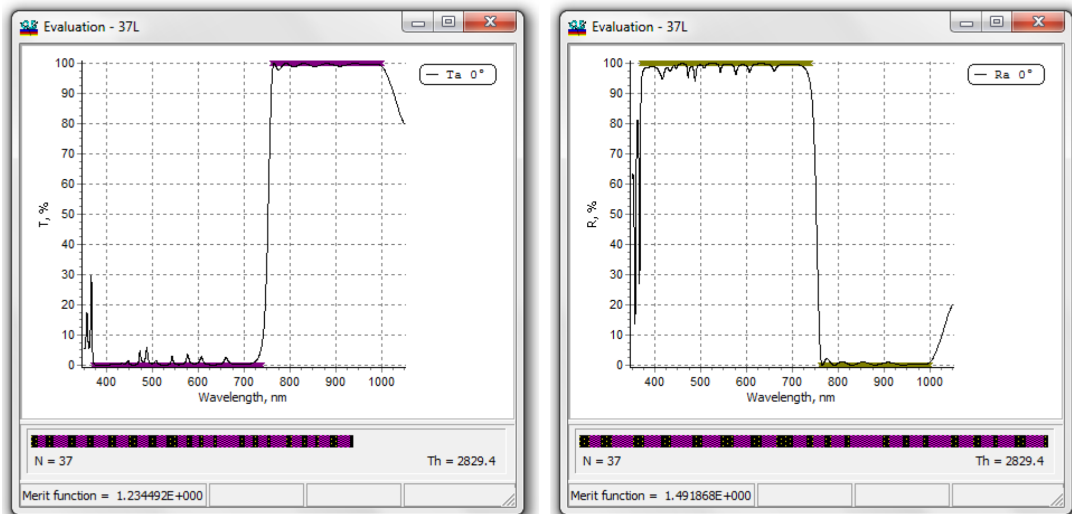

Figure 5.18: 37-layer design for long-pass filter

(the left is transmission and the right is reflection curve)

Again a backside coating is needed to minimize the backside reflection. The backside effect on the current design and the transmission curve after backside coating design are shown in the Figure 5.19 and 5.20, respectively.

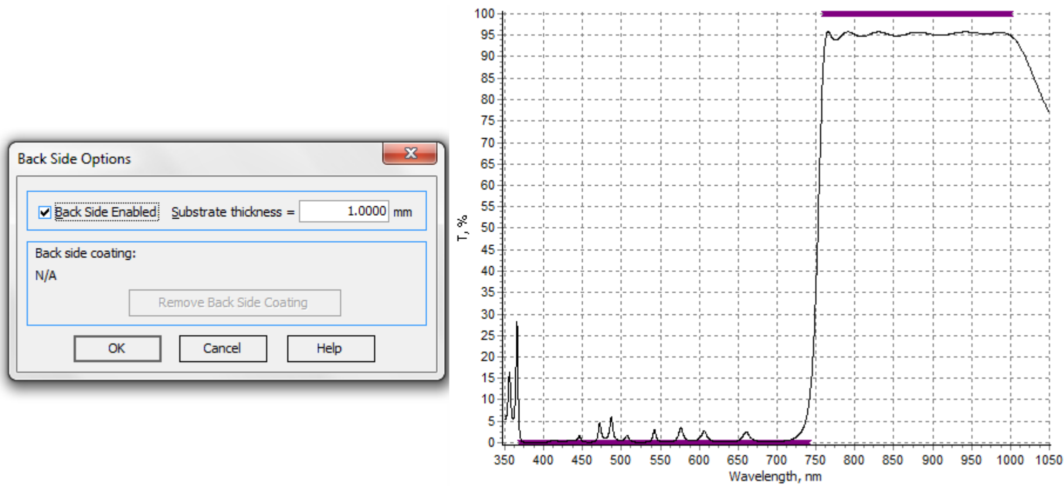

Figure 5.19: Effect of backside reflection

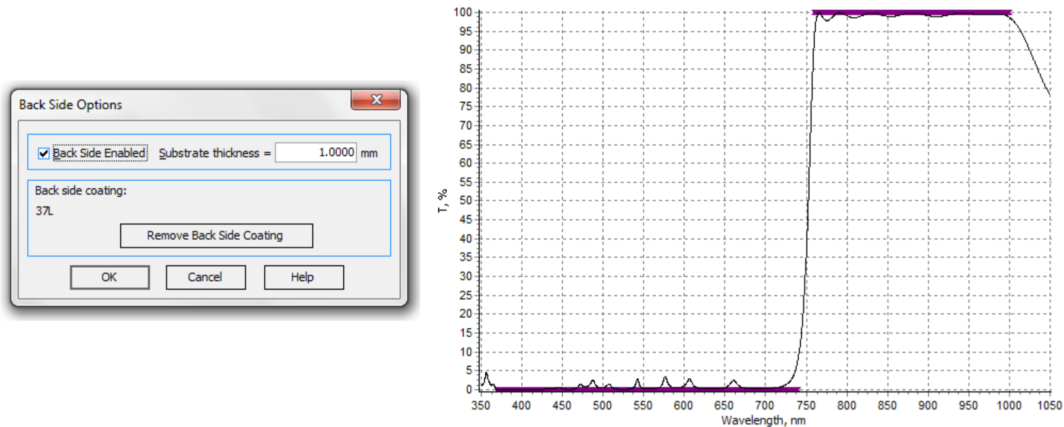

Figure 5.20: Final design for long-pass filter

5.4 Production of Filters

5.4.1 The Coating Process

After the designs are completed, the production process can start. For filters, the glass was cut by laser to fit the CCD surface as shown in the Figure 5.21.

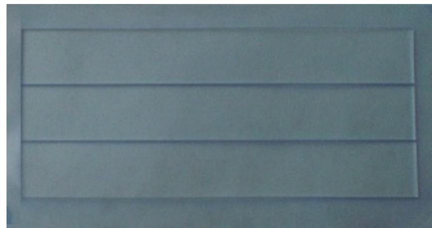

Figure 5.21: Filter glasses

In order to install the glasses into the vacuum chamber, a new holder should be produced. Figure 5.22 shows the holder produced for this reason. Three filter glasses can be coated by this holder in one process.

Figure 5.22: Holder for filter glasses

Since the glasses do not have any contamination from polishing process and the coating process has an etching (in-situ cleaning) step, the surface cleaning can be done by pure acetone under fluorescent lamp. In this method, the cleaning should be done by more than one step because the small particles (dust) from surface may mix up into the acetone in each try and

they may stick to the surface again. Therefore, 3-beaker acetone was used; the first one is for rough cleaning, the second is for precise cleaning and the third is for final cleaning. If necessary, compressed air can be used to blow the last remaining particles. The substrates should put into the vacuum chamber immediately after the cleaning process.

The designs should be loaded to the coating system. In the thickness control, both OMS and XMS can be used simultaneously. In this way, OMS makes calculations and gives warning massages if something goes wrong but stop condition is determined by quartz crystal system. For XMS, the tooling factors found for coating materials should be entered as process parameters. For OMS, the control wavelength should be determined by the contribution of $tooling_{O}MS$ in order to make correct calculation as mentioned in Chapter 4. Figures 5.23 and 5.24 show the monitoring page of OptiLayer in which tooling factors was loaded and suitable control wavelengths was chosen.

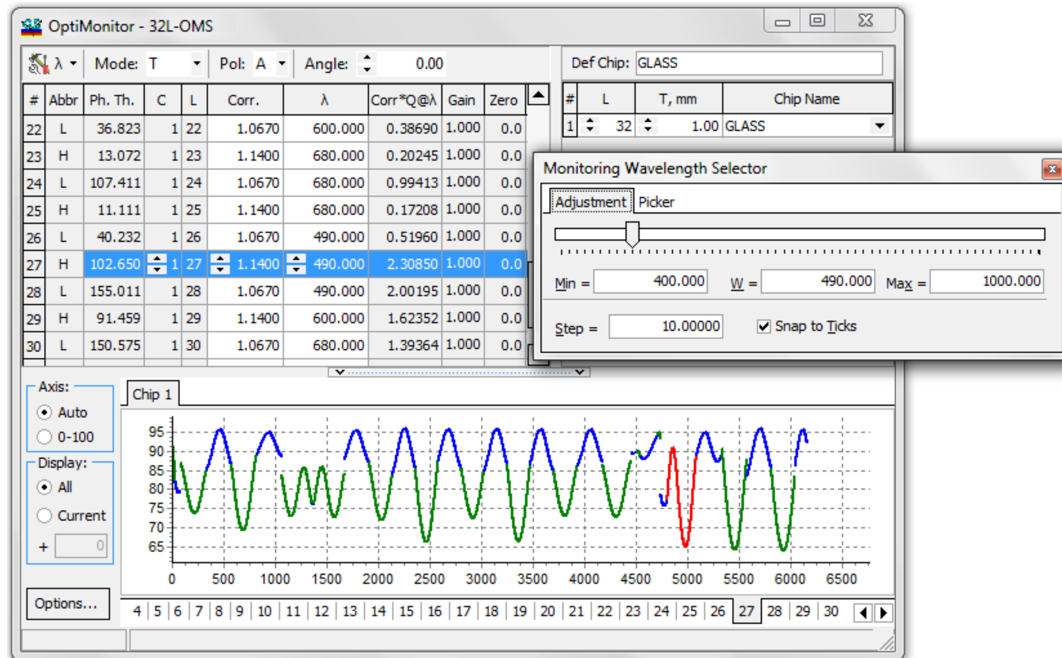

Figure 5.23: Monitoring for short-pass filter

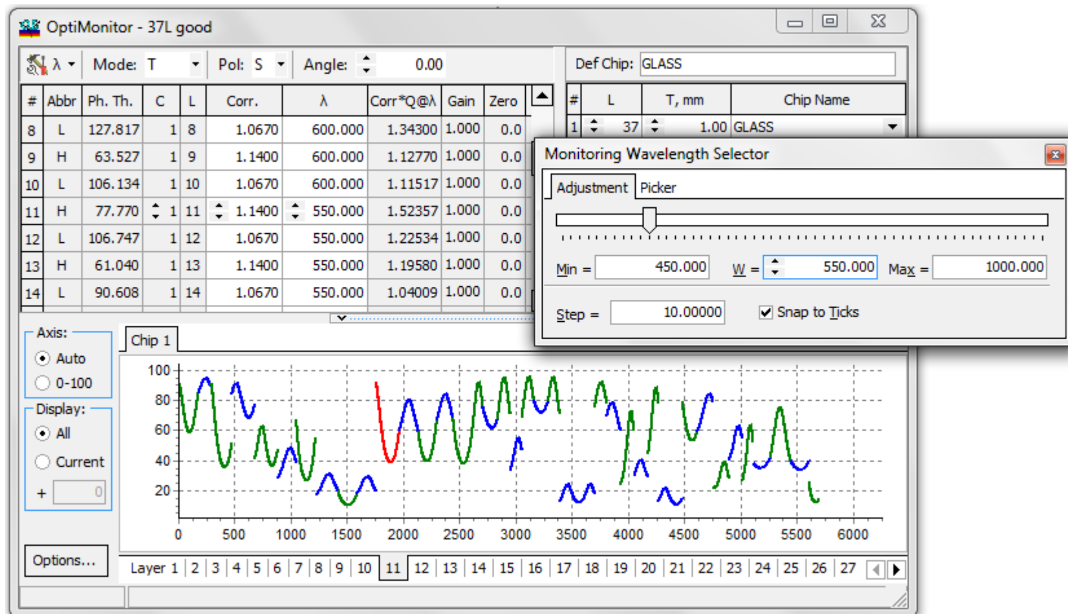

Figure 5.24: Monitoring for long-pass filter

Before the production, homogeneity mask was chosen to make the coating homogenous along the whole surface and Ti_3O_5 target material was melted (pre-melt process). After whole these pre-work, the coating process can start. Each process starts when the starting pressure is achieved (10^{-5} mbar) and includes heating and etching steps before the coating begins.

5.4.2 Spectroscopic Measurements

The spectroscopic measurements of the filters were made by the UV/Vis spectroscopy.

5.4.2.1 The Spectrophotometer: Perkin Elmer - Lambda 950

The Lambda 950 is an instrument that operates in the ultraviolet (UV), visible (Vis) and near-infrared (NIR) spectral ranges (between 175-3300 nm). The optical system in the spectrophotometer is shown schematically in Figure 5.25.

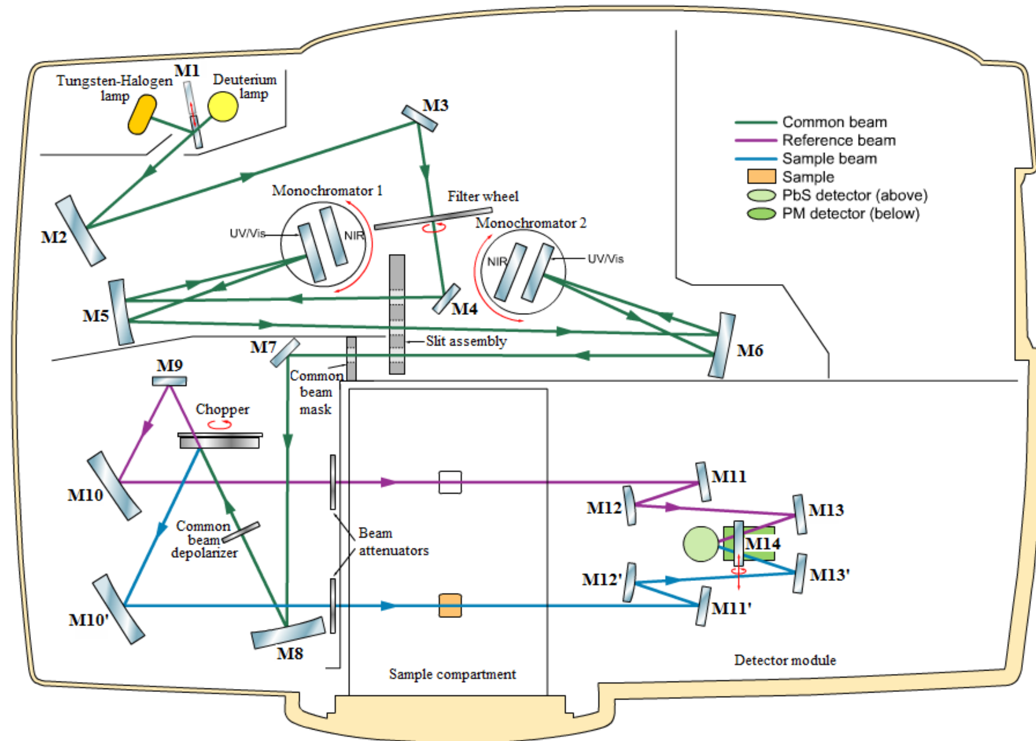

Figure 5.25: Schematic diagram of the optical system in spectrophotometer.

To cover the whole wavelength range, two radiation sources, a halogen lamp (for NIR and Vis ranges) and a deuterium lamp (for UV range), are used. The movable mirror M1 is used to select one of these sources and block the other. The path followed by the radiation is shown in Figure 5.25. The radiation reflected from mirrors M2 and M3 passes through an optical filter on the filter wheel that is in synchronization with monochromators. The radiation is prefiltered by the appropriate optical filter that is placed in the beam path depending upon the wavelength being produced.

The beam reflects from mirror M4, passes through the entrance slit of the first monochromator and reflected to the grating table by mirror M5. The beam hits either the UV/Vis grating or NIR grating according to the current wavelength range and is dispersed to produce a spectrum. A segment of the spectrum selected by the rotational position of the grating strikes the mirror M5 again and passes through the exit slit which makes this segment near-monochromatic. Then, the radiation is reflected to the second monochromator via mirror M6 and continues to follow the path shown in the figure. The rotational gratings tables of monochromator 1 and

monochromator 2 are in synchronization. The radiation after exit slit displays high spectral purity. A common beam mask restricts the cross-section of the beam.

Then, the radiation strikes the mirror M7 and M8 and is reflected to the chopper which includes a window segment, a mirror segment and two dark segments. By the help of chopper, reference beam, sample beam and dark signal are created. After reflecting from a series of mirrors, the reference and sample beams reach the appropriate detector. There are two detectors in the system; a photomultiplier (PM) for UV/Vis range and a lead sulfide detector (PbS) for NIR range. The mirror M14 is used to select the required detector.

5.4.2.2 The Measurement Results

The results of the measurements done by Perkin-Elmer Lambda950 spectrophotometer are shown below. Figure 5.26 shows transmission measurement of short-pass filter with single side coating.

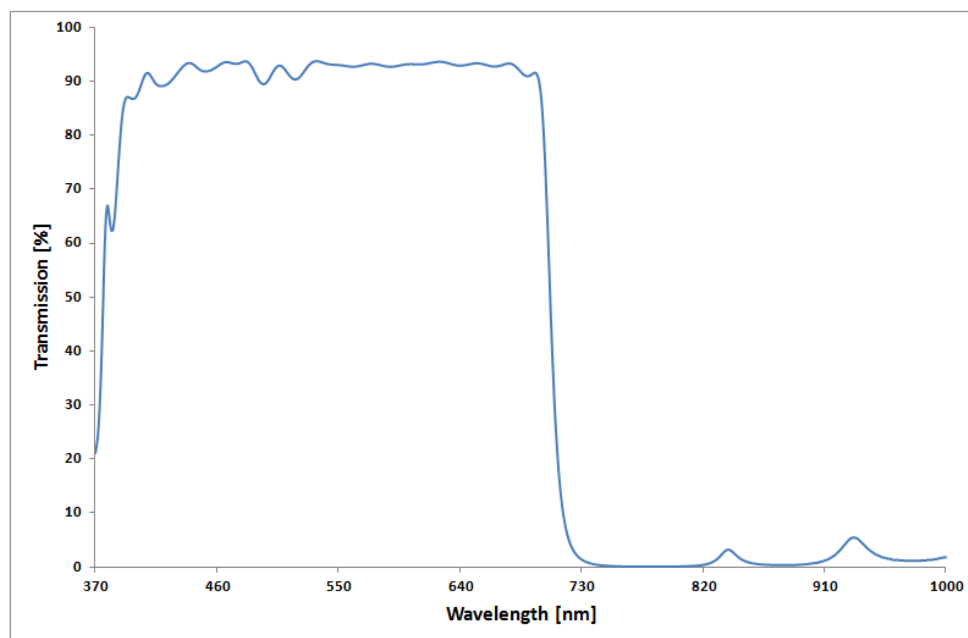

Figure 5.26: Single side coated short-pass filter

After backside coating, the transmission curve of the short-pass filter is shown in Figure 5.27.

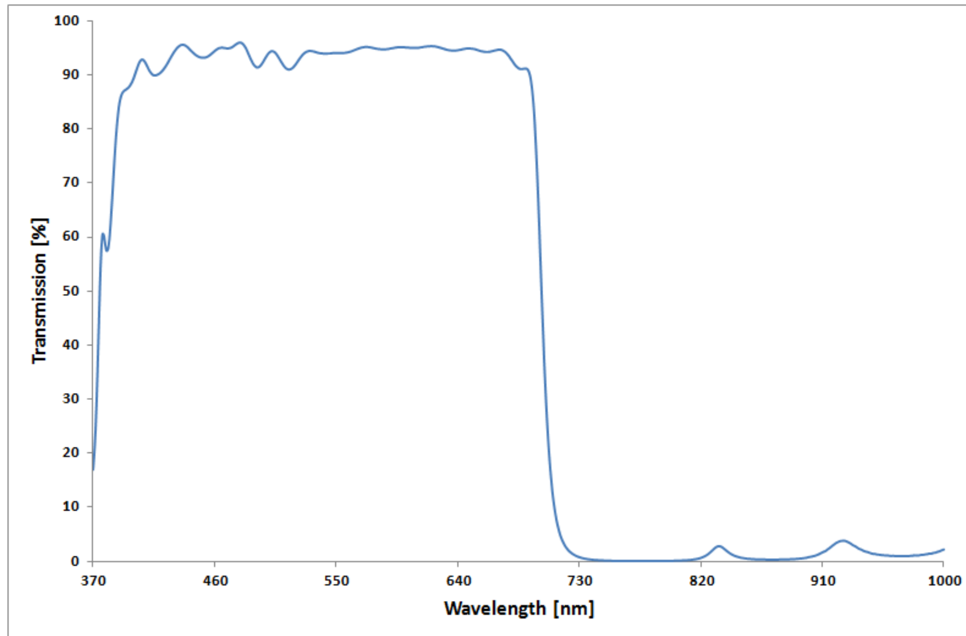

Figure 5.27: Short-pass filter with backside coating

The transmission curves belonging to the long-pass filter are shown in Figure 5.28 (single side-coated) and Figure 5.29 (two-side coated).

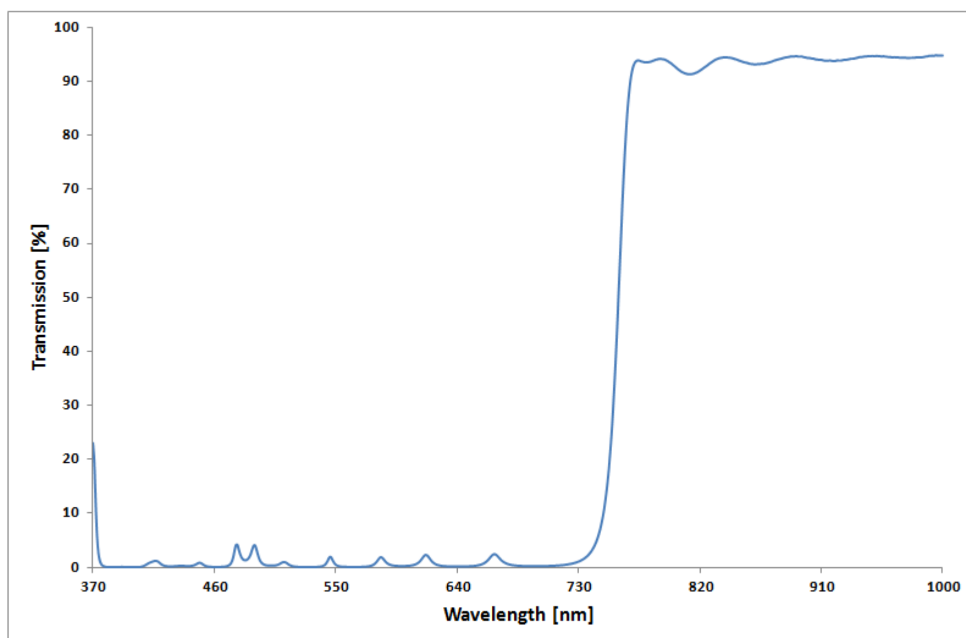

Figure 5.28: Single side coated long-pass filter

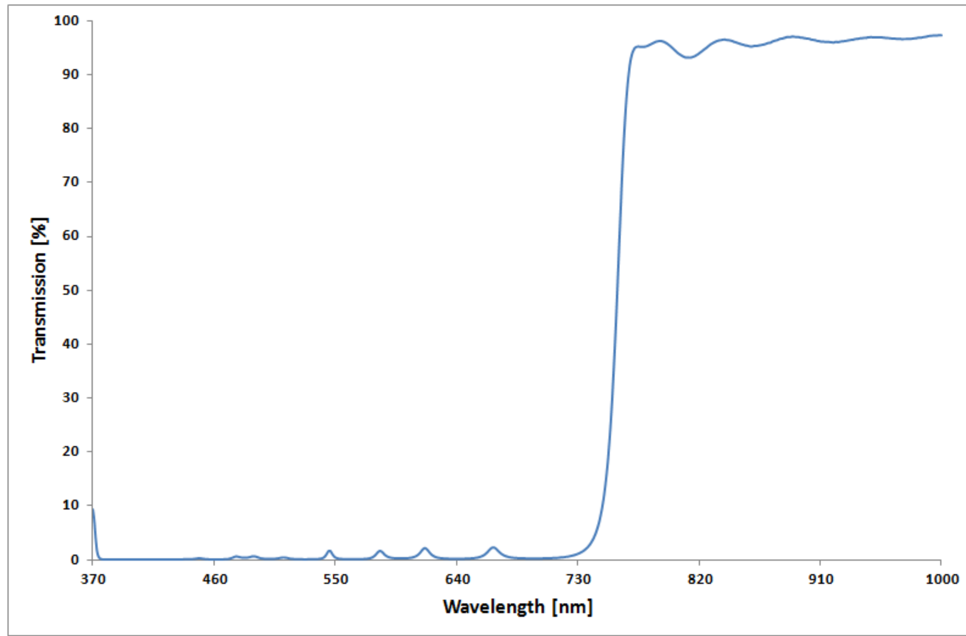

Figure 5.29: Long-pass filter with backside coating

CHAPTER 6

CONCLUSION

The optical coatings are used in many applications. The property of an optical surface can be altered in the desired way by optical coatings. The reflectivity can be increased or decreased for a region or the undesired part of the spectrum can be filtered. In this thesis, two optical edge filters have been produced. The wavelength spectrum includes the range between $370 - 1050$ nm. The main purpose of this work is to divide this spectrum into two parts in order to obtain images in two bands; RGB and NIR, by charge-coupled devices.

In this thesis, after general information about image sensors and charge-coupled devices have been given, the theory of thin film and the basics of optical coatings have been studied. Thin film deposition techniques have been examined and the system SyrusPro1110, used in the production of filters, has been explained in detail.

As layer materials, SiO_2 and TiO_2 have been chosen and as target material SiO_2 and Ti_3O_5 was used. In order to achieve the same results with the design, the optical properties of all constituents should be known. Therefore, before the design procedure, the wavelength-dependent refractive indices and the tooling factors belonging to the coating materials have been calculated by means of single layer coatings. The obtained results for refractive indices have been loaded in design program to define the coating materials, and tooling factors have been loaded to the coating system to control the layer thicknesses in a correct way.

The filters have been designed by the program OptiLayer and produced by plasma ion-assisted deposition technique. The design procedure, including many optimization and refinement steps, was ended with acceptable optimum solution. To be ready for production, premelt process of Ti_3O_5 target material has been done, homogeneity studies were conducted to select

or form homogeneity mask and substrates have been cleaned. In production, B270 glass substrates were coated by e-beam evaporation of the materials under the vacuum with a pressure about 9.8×10^{-6} mbar. With back side coatings, both the transmittance in the transmission zone was increased by %2-3 and the ripples in the reflection zone were reduced. The thickness control of the layers has been done by using two systems; OMS and XMS. After production, the transmission properties of filters have been measured with Perkin Elmer, Lambda 950 Spectrophotometer. The results are very similar to the designs. The little difference can be caused from some production parameters. Since a material has different tooling factors at different thicknesses, using same tooling factor for all layers including too thin ones can affect the resultant coating. In addition, the rate of SiO_2 is not stable since it directly sublimates. Therefore, the thickness measurements of thin SiO_2 ($\sim 7-8$ nm) layers can cause some problems. Furthermore, during the process, not only the substrates but also the components and the walls of the coating machine are coated. Therefore, for multilayer coatings, this situation can affect the quality of the coating. However, when the measurement results are compared with the designs, there is not unacceptable difference between them. The specifications of produced filters are shown in the table below.

Table 6.1: Specifications of produced optical filters

SPECIFICATIONS	**Short - Pass Filter**	**Long - Pass Filter**
Dimensions	60 mm × 9 mm × 1 mm	60 mm × 9 mm × 1 mm
Layer Materials	SiO_2 & TiO_2	SiO_2 & TiO_2
Number of Layers	32	37
Number of Layers (Back Side)	9	15
Total Coating Thickness	2979.2 nm 821.61 nm (Back Side Coating)	2829.4 nm 889.16 nm (Back Side Coating)
Angle of Incidence	Normal	Normal
Spectral Range	370 – 1000 nm	370 – 1000 nm
Rejection (Spectral)	710 – 1000 nm	370 – 740 nm
Transmittance Range	370 – 690 nm	760 – 1000 nm
T_{AV} (transmittance range)	91.3 %	95.3 %

Figure 1.4 given in the chapter 1 shows the responsivity curve of KLI 4104 CCD. When the responsivity curves for red, green and blue channels are multiplied with the transmission curves of produced filters, the final graphs give the responsivity curves of CCD - filter combination. Figure 6.1 shows the resposivity curve of CCD with short-pass filter and Figure 6.2 shows the resposivity curve of CCD with long-pass filter.

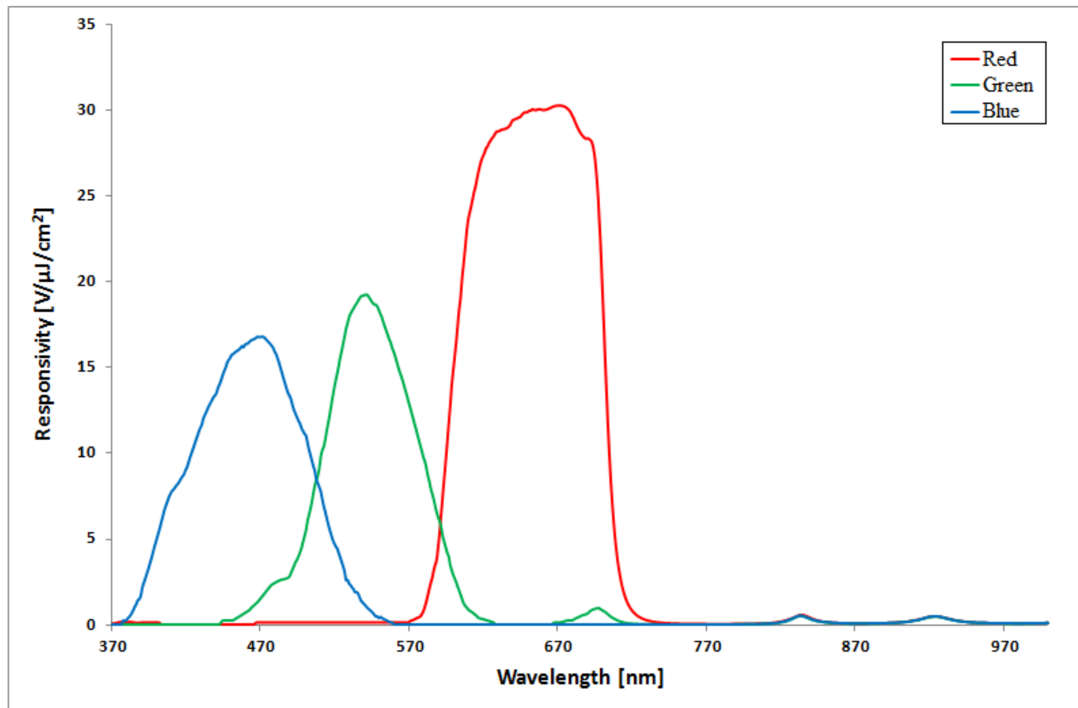

Figure 6.1: Responsivity curve of CCD with short-pass filter.

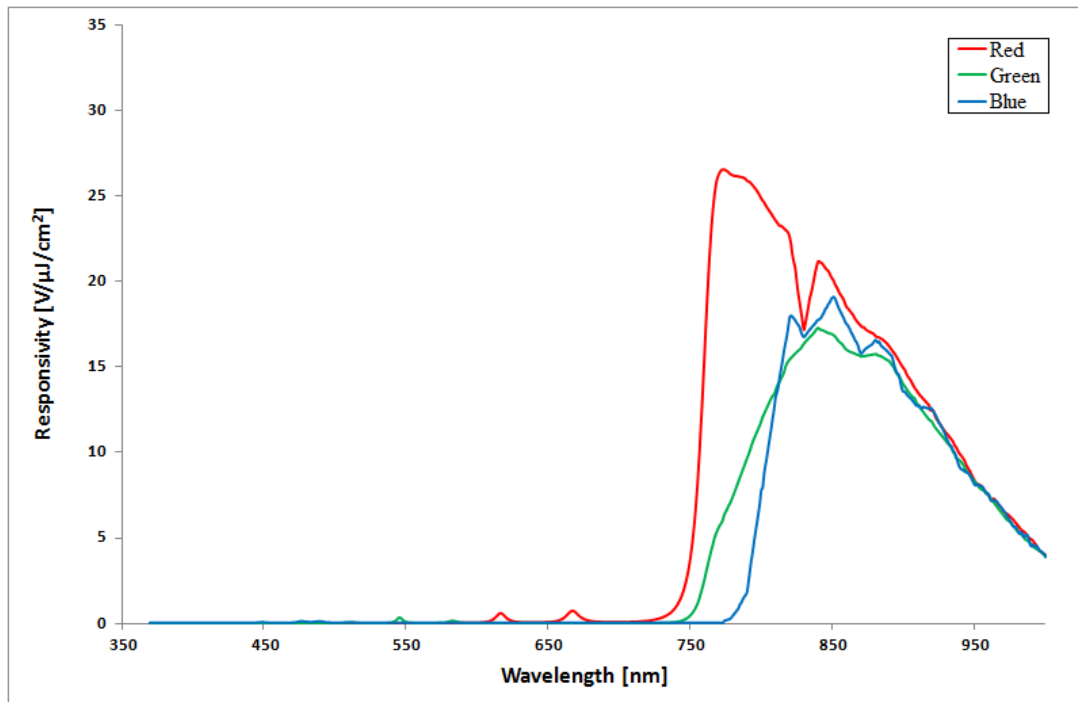

Figure 6.2: Resposivity curve of CCD with long-pass filter.

While RGB image can be obtained with CCD + short-pass filter, the image in the NIR range can be obtained with CCD + long-pass filter by using one of the red, green or blue channels.

In summary, in this thesis, a 32-layer short-pass filter and a 37-layer long-pass filter that divide the 370 - 1050 nm spectrum into two bands have been designed and produced. The transmission has reached > 90% in the transmission zone and the reflection has reached > 95% in the filtered zone with backside coatings. These filters have been used in the electronic unit of a space camera. In the electronic unit, three KLI-4104 sensors have been used to obtain PAN, RGB and NIR images. For panchromatic imaging, an uncoated glass has been placed on one of the sensors while short-pass filter and long-pass filter have been used for RGB and NIR images, respectively. In this way, imaging in different regions can be achieved by using same CCDs.

REFERENCES

[1] Knittl, Z. *Optics of Thin Films*, John Wiley & Sons, Czechoslovakia, 1976.

[2] Newport Thin Film Laboratory, *www.newportlab.com*, [last accessed date: 03.07.2012]

[3] Application Note:A003, *Optical Thin Film Applications*, [online], *http://www.opto.com.sg/downloads/optical%20thin%20film%20applications.pdf*.

[4] Chromey, F. C., *To Measure the Sky: An Introduction to Observational Astronomy*, Cambridge University Press, New York, 2010.

[5] Thelen, A. *Design of Optical Interference Coatings*, McGraw-Hill, 1989.

[6] Optical Coatings, *www.cvimellesgriot.com*, [last accessed date: 02.05.2011]

[7] Wasa, K., Kitabatake, M., & Adachi, H., *Thin Film Materials Technology: Sputtering of Compound Materials*, Springer, United States, 2004.

[8] Pedrotti, F. L., Pedrotti, L. S., & Pedrotti, L. M., *Introduction to Optics*, Prentice Hall, New Jersey, 2007.

[9] Mattox, D. M., *Handbook of Physical Vapor Deposition (PVD) Processing*, William Andrew, Oxford, UK, 2010.

[10] Pierson, H. O., *Handbook of Chemical Vapor Depostion (CVD) : Principles, Technology, and Applications* , Noyes Publications, Norwich, N.Y., 1999.

[11] Zöller, A., Beibwenger, S., Götzelmann, R. & Matl, K., *Plasma ion assisted deposition: A novel technique for the production of optical coatings*, SPIE Vol.2253, 394-402

[12] Prabhakara, H. R., *Plasma Assisted Physical Vapour Deposition*, [online], http://bangaloreplasmatek.com/plasma.pdf.

[13] Midwest Tungsten Service *http://www.tungsten.com/tipsbeam.pdf*, [last accessed date: 03.07.2012]

[14] Zöller, A., Götzelmann, R., Matl, K. & Cushing, D., *Temperature-stable bandpass filters deposited with plasma ion-assisted deposition*, Applied Optics, Vol.35, No.28, 5609-5612, 1996.

[15] Operating Instructions, *SyrusPro1110 Evaporation system for creating optical coatings*, Leybold Optics, Edition: 04/2008_V6_1_en.

[16] Willey, R. R., *Practical Design and Production of Optical Thin Films*, Marcel Dekker Inc, New York, 2002.

[17] Eroğlu, C., *Design of Reflective and Antireflective Coatings for Space Applications*, Ms. Thesis, 2009.

[18] Friz, M., & Waibel, F., *Coating Materials*, [online], *http://www.tsvacuum.com/spanish/UploadFiles/200813112542318.pdf*.

[19] Macleod, H. A., *Thin Film Optical Filters*, CRC Press, Arizona, USA, 2010.

[20] Pedrotti, F. L., Pedrotti, L. S. & Pedrotti, L. M., *Introduction to Optics*, Prentice Hall, New Jersey, 2007.

[21] Jones, A. C., Hitchman, M. L., *Overview of Chemical Vapour Deposition*, Jones, A. C.(Ed.), Hitchman, M. L. (Ed.), Chemical vapour deposition: precursors, processes and applications. (1-36), RSC Publishing, UK, 2009.

[22] Nishi, Y., Doering, Y., *Handbook of Semiconductor Manufacturing Technology*, Marcel Dekker, New York, 2000.

[23] Howel, S. B., *Handbook of CCD Astronomy*, Cambridge University Press, New York, 2006.

[24] KODAK Solid State Image Sensor Terminology *http://www.kodak.com/ek/uploadedFiles/terminology(1).pdf*, [last accessed date: 03.07.2012]

[25] Willey, R. R., *Practical Design and Production of Optical Thin Films*, Marcel Dekker INC., USA, 2002.

[26] Pongratz, S., Zöller, A., *Plasma ion-assisted depositon: A promising technique for optical coatings*, American Vacuum Society, Vol.10, No.4, 1897-1904, 1992.

[27] Grimshaw, S., *Temperature Measurement and Control of Quartz Crystal Microbalances*, Tangidyne Corp, 2007.

[28] Schallenberg, U. B., *Steep-edge filter design with equivalent layers*, SPIE Vol.5963, 2005.

APPENDIX A

WAVELENGTH-DEPENDENT REFRACTIVE INDEX of B270

Table A.1: Dispersion Data of B270 Glass (obtained from manufacturer)

Wavelength [nm]	Refractive Index (n)	Wavelength [nm]	Refractive Index (n)
350	1.559636	495	1.526481
355	1.557341	500	1.52599
360	1.555191	505	1.52552
365	1.553173	510	1.52507
370	1.551278	515	1.524639
375	1.549496	520	1.524225
380	1.54782	525	1.523828
385	1.546241	530	1.523447
390	1.544752	535	1.523081
395	1.543348	540	1.522729
400	1.542021	545	1.522391
405	1.540768	550	1.522066
410	1.539582	555	1.521753
415	1.53846	560	1.521452
420	1.537396	565	1.521162
425	1.536388	570	1.520882
430	1.535432	575	1.520613
435	1.534524	580	1.520354
440	1.533661	585	1.520103
445	1.53284	590	1.519862
450	1.53206	595	1.519629
455	1.531317	600	1.519404
460	1.530609	605	1.519186
465	1.529934	610	1.518976
470	1.52929	615	1.518773
475	1.528676	620	1.518577
480	1.52809	625	1.518387
485	1.527529	630	1.518203
490	1.526993	635	1.518025

Wavelength [nm]	Refractive Index (n)	Wavelength [nm]	Refractive Index (n)
640	1.517853	830	1.513947
645	1.517686	835	1.513887
650	1.517525	840	1.513829
655	1.517368	845	1.513772
660	1.517216	850	1.513716
665	1.517069	855	1.513662
670	1.516927	860	1.513608
675	1.516788	865	1.513556
680	1.516654	870	1.513505
685	1.516523	875	1.513455
690	1.516397	880	1.513406
695	1.516274	885	1.513359
700	1.516154	890	1.513312
705	1.516038	895	1.513266
710	1.515925	900	1.513221
715	1.515815	905	1.513177
720	1.515709	910	1.513134
725	1.515605	915	1.513092
730	1.515504	920	1.513051
735	1.515405	925	1.51301
740	1.51531	930	1.512971
745	1.515217	935	1.512932
750	1.515126	940	1.512894
755	1.515037	945	1.512857
760	1.514951	950	1.51282
765	1.514867	955	1.512784
770	1.514786	960	1.512749
775	1.514706	965	1.512714
780	1.514628	970	1.51268
785	1.514552	975	1.512647
790	1.514478	980	1.512615
795	1.514406	985	1.512583
800	1.514336	990	1.512551
805	1.514267	995	1.51252
810	1.5142	1000	1.51249
815	1.514134	1005	1.51246
820	1.51407	1010	1.512431
825	1.514008	1015	1.512402